Ionic Flexible Sensors: Mechanisms, Materials, Structures and Applications

Chun Zhao [a,1], Yanjie Wang[a,1]*, Gangqiang Tang[a], Jie Ru[a], Zicai Zhu[b], Bo Li[b], Chuan Fei Guo[c], Lijie Li[d], Denglin Zhu[a]

[a] *Jiangsu Provincial Key Laboratory of Special Robot Technology, Hohai University, Changzhou campus, Changzhou, 213022, China*

[b] *School of Mechanical Engineering, Xi'an Jiaotong University, Xi'an, Shaanxi 710049, China.*

[c] *Department of Materials Science and Engineering, Southern University of Science and Technology, Shenzhen, 518055 China.*

[d] *College of Engineering, Swansea University, Swansea, SA1 8EN, UK*

Email: yj.wang1985@gmail.com

Abstract:

Over the past few decades, the flexible sensors have been developed from the "electronic" level to the "iontronic" level and then gradually to the "ionic" level recently. Ionic Flexible Sensors (IFS) represents one kind of advanced sensors based on ion migration. Compared with conventional electronic sensors, IFS not only replicate the topological structures of human skin, but also have the potential to achieve tactile perception functions like skin of human being, which provide powerful tools and methods for narrowing the gap between conventional electronics and biological interface. In this paper, the latest research and developments about several typical sensing mechanisms, the compositions, structural design and applications of IFS are comprehensively reviewed. In particular, the development of novel ionic materials, structural designs and biomimetic approaches have given birth to a wide range of novel and exciting IFS, which can not only effectively sense pressure, strain, humidity with high sensitivity and high reliability, but also have self-powered, self-healing, biodegradability and other properties of human skin. Furthermore, the typical applications of

IFS in artificial skin, human-interactive technologies, wearable health monitors and other related fields are reviewed. Last, perspectives on the current challenges and future directions of this field are presented.

Keywords: ionic polymer, flexible sensors, sensing mechanisms, electrodes, structures

1. Introduction

Tactile perception is one of the main functions for human being to perceive external environment. In recent decades, inspired by mimic this natural perception ability, flexible sensors have undergone rapid developments and have attracted considerable attention from academia and industry. Compared with conventional rigid sensors, flexible sensors are endowed with distinguished properties, such as stretchability, deformability, super-hydrophilicity and biocompatibility, which have shown extremely broad application prospects in human-interactive technologies, medical monitoring, and electronic skins.

Flexible sensors are usually composed of multiplayer matrix materials and electrodes. According to the intrinsic characteristics of matrix materials, the mechano-electric transforming mechanisms of current flexible sensors can be categorized into piezoelectric, piezoresistive, and ionic types. The sensing signaling of piezoelectric and piezoresistive sensors are mediated by electrons. Piezoelectric sensors usually use piezoelectric materials as matrix which converts mechanical strains into electrical signals. The piezoelectric effect can be explained by dipole deflection within the material. When subjected to external mechanical strain, the deformation of crystal structure in the material leads to polarization. The originally chaotic dipoles present a regular sequence under external mechanical stress, which will form dipole moments at both surfaces of the material and generate electrical signals [1]. General flexible piezoresistive materials are composed of polymer matrixes and conducting fillers. When the volume content of the conducting filler increases (i.e. the pressure increases), the average distance between the conducting particles will shorten, which will form new conducting path to reduce the resistivity [2]. This kind of flexible sensors has good sensitivity at a certain stretching range. Unfortunately, whether it is piezoelectric or piezoresistive sensors, it has a high Young's modulus and a very narrow strain range (< 10%) due to the strong chemical bonding force between the molecular structures [3, 4]. Nevertheless, It is reported that the human skin at joints allows the strain more than 30% [5], at least several orders of magnitude lower than that of piezoelectric and piezoresistive materials. In addition, since biological signaling is mediated by ions, the intimate communication between piezoelectric or piezoresistive electronic sensors and biological systems exists a technological

challenge.

In contrast to electronic systems, human skin rarely uses electrons as the signal to sense external stimuli, but rather ions and molecules. According to biology, in the equilibrium state, the biological ion channels in human skin are closed, and the concentrations of cations and anions inside and outside the cell membrane are kept in balance. When subjected to external stimuli, the ion channels on the cell membrane are opened, and the Na^+ in the extracellular matrix flows into the cell, thereby generating electrical signals to the nervous system for sensing external stimuli, such as pressure, strain, temperature, humidity, etc. In the past few years, the sensing mechanism of human skin has been mimicked by IFS that rely on the electron-mediated transport and compensation of ions. When IFS is in the equilibrium state, anions and cations are evenly dispersed in the ionic electrolyte. When subjected to external stimuli, the anions and cations separately migrate to both sides of IFS to form an electrical signal. IFS not only replicates the tactile functions and topological structures of human skin, but also mimics the biological sensing mechanism based on the ion migration, and hence represent great conceptual similarities with biological systems. In particular, recently, bio-inspired methods can provide an opportunity to create some IFS with higher sensitivity and broader pressure response range beyond those of human skin. This means deformable ionic sensor devices that can sense various external stimuli has been introduced to mimic the tactile perception of human skin more closely. IFS are usually composed of electrode layers and the ionic polymer matrix. A solid ionic polymer matrix usually contains polymer matrix and ionic electrolyte. The former make the ionic polymer matrix hold the appropriate stiffness while the latter makes the matrix keep moderate electrical conductivity and obtain movable ions. The nanopores of polymer matrix are usually much larger than that of water molecules and ions, so that the movable ions move freely in the polymer. Under the stimulation of mechanical force, the ions will redistribute and form an electric double layer at the interface between ionic polymer matrix and electrodes [6]. As early as 2011, *Pan et al.* firstly reported a pressure sensor, which forms a supercapacitor with an electric double layer by loading ionic droplets on the surface of chemically modified electrodes [7, 8]. Different from the previous piezoelectric and piezoresistive electronic sensors, this liquid-solid structure of IFS has a very low Young's modulus and exhibits better biocompatibility with high sensitivity. Since then,

many researchers have tried to use a variety of ionic matrixes, including ionic liquids [9-11], polyelectrolytes [12-15], and ionic gels [16-18], to prepare IFS for tactile perception. The IFS can successfully respond to a variety of external stimuli, such as pressure [19-21], strain [22, 23], torsion [24], and tangential force [10].

Despite lots of efforts have been made to mirror the topological microstructure of human skin into the IFS, most IFS only rest on the flexible sensor from “electron” level to “iontronic” level (because the electrode belongs to “electron” level). However, there are only ions as a signaling medium in the human body, which is still a crucial technical challenge for the development of biocompatible IFS. Recently, various new ionic polymer matrixes and ionic conductive electrodes have been developed to realize ionic mechanotrans-duction phenomena across biological ion channels that can be observed in human skin. Compared with electronic and iontronic skin devices, it abandons the concept of electronic conduction and only uses "ions" to realize signal generation and conduction, showing a more advanced biological interface. In addition, to completely mimic the properties of human skin, IFS with self-powered, self-healing, biodegradability and other properties of human skin has also been developed recently. These significant progresses in the IFS make them a wonderful candidate for emerging technologies in the field of wearable or bio-inspired sensor platforms.

Herein, in this review, we will survey the state-of-the-art progress on IFS, with in-depth discussions on the theoretical sensing models, ionic polymer matrixes, stretchable flexible electrodes, structural design and applications, the current challenges and prospective trends, as shown in **Figure 1**. The organization of this review is as follows. In Section 2, we will introduce the sensing mechanisms and theoretical sensing models of IFS, including supercapacitive interfacial IFS, piezoelectric IFS and piezoresistive IFS. Then, in Section 3, we summarize the up-to-date developments and research trends of the ionic polymer matrix for IFS, including ionic gels, polyelectrolytes and other ionic materials. After that, we discuss the latest research on stretchable flexible electrodes, including metal electrodes, non-metal electrodes. The latest research on the structure design of IFS will be discussed in Section 4, including surface structure and internal structure. Subsequently, novel applications based on ionic flexible sensors will be shown in Section 5, such as artificial skin, human-interactive technologies, and wearable medical devices. Finally, we will make a comment on the current

challenges and the prospective trends of IFS, which provides a future technical roadmap for innovation and breakthroughs in this emerging area.

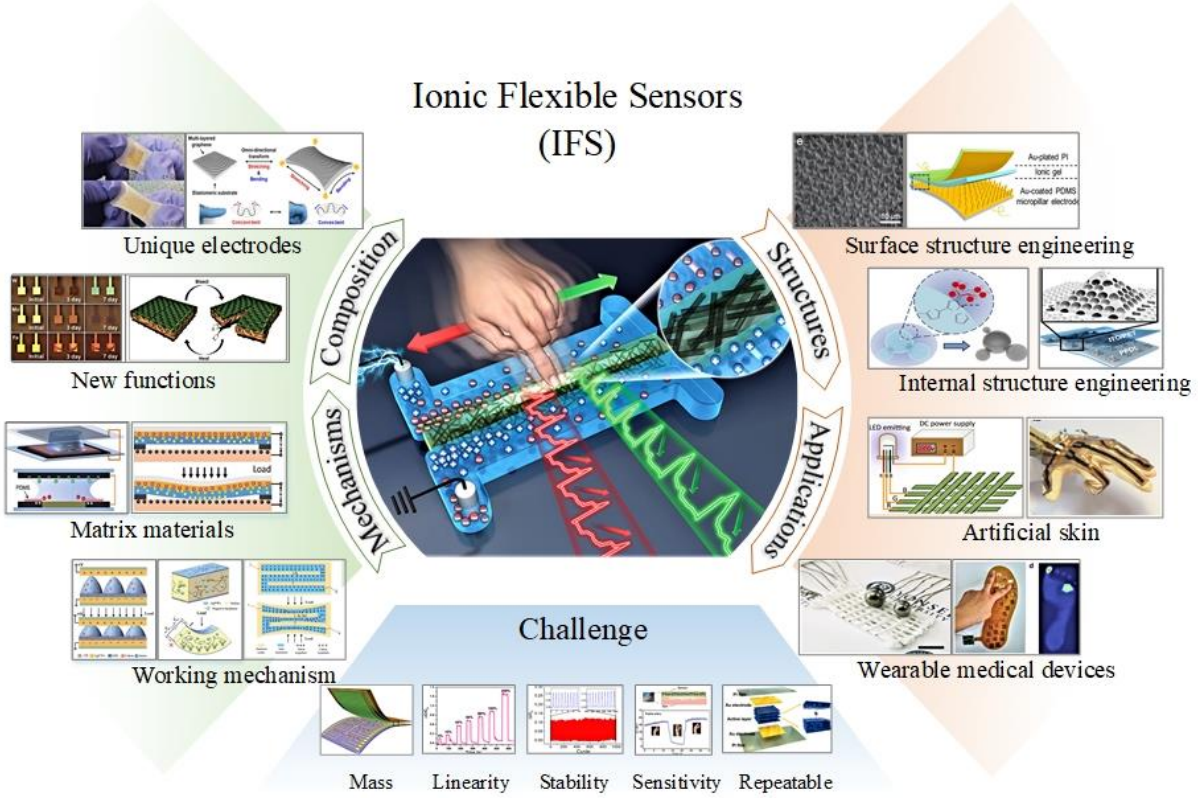

Figure 1. Mechanisms, composition, structures, applications of ionic flexible sensors (IFS). Working mechanism: Reproduced with permission.[82] Copyright 2018, Wiley-VCH. Matrix materials: Reproduced with permission.[30] Copyright 2020, Wiley-VCH. Reproduced with permission.[127] Copyright 2018, Wiley-VCH. New functions: Reproduced with permission.[110] Copyright 2017, Wiley-VCH. Reproduced with permission.[121] Copyright 2019, Elsevier. Unique electrodes: Reproduced with permission.[192] Copyright 2014, Wiley-VCH. Reproduced with permission.[164] Copyright 2016, American Chemical Society. Surface structure engineering: Reproduced with permission.[233] Copyright 2018, Wiley-VCH. Reproduced with permission.[241] Copyright 2021, Elsevier. Internal structure engineering: Reproduced with permission.[248] Copyright 2016, American Chemical Society. Reproduced with permission.[250] Copyright 2019, American Chemical Society. Artificial skin: Reproduced with permission.[249] Copyright 2016, Royal Society of Chemistry. Reproduced with permission.[269] Copyright 2018, Wiley-VCH. Wearable medical devices: Reproduced with permission.[270] Copyright 2015, Wiley-VCH. Reproduced with permission.[285] Copyright 2018, Wiley-VCH. Mass production: Reproduced with permission.[79] Copyright 2020,

Wiley-VCH. Stability: Reproduced with permission.[232] Copyright 2021, Elsevier. Sensitivity: Reproduced with permission.[246] Copyright 2020, Wiley-VCH. Repeatable: Reproduced with permission.[292] Copyright 2021, American Chemical Society.

2. Ionic sensing mechanisms

Different to other sensors, IFS usually transform the external mechanical strain into the electrical signal by internal ion migration. After years of development, researchers have developed different types of IFS, including supercapacitive interfacial IFS, siezoelectric IFS and siezoresistive IFS, and have carried out extensive research on their transduction mechanisms. In this section, we will describe various ionic transduction mechanisms, and discuss their fundamental transduction models and key influencing factors.

2.1 Supercapacitive interface effect

The inception of supercapacitive interfacial sensing has been intriguing in fact, which originates from a long-known interfacial effect, electronic double layer (EDL), in electrochemistry [25]. Thanks to the development of superhydrophobic chemistry, microfluidics and flexible electronics, supercapacitive interfacial IFS could be initially formed by direct contact between ionic liquid and electrodes [26]. These IFS present a very high sensitivity, the capacitive values of which will change significantly when subjecting to a slight external mechanical force. Compared with the conventional capacitive sensors, supercapacitive interfacial IFS based on electric double-layer (EDL) can produce an ultrahigh capacitance per unit area up to several μF cm^{-2} in sub-MHz spectrum, where the capacitive value increased more than 1000 times [30]. In general, the electrode with excess carriers will generate strong electrostatic force. When the ionic material (solid or liquid) contacts with the electronic conductor (i.e. electrode), the charged electronic conductor will repel the ions with the same charge, while the ions with opposite charge will be attracted to the electrode surface, and then the EDL is formed at the interface between the ionic material and the electronic conductor. However, ionic liquids have high liquidity, which will cause some unavoidable problems, such as low durability and complicated capsulation technology [27-30]. According to the sensing mechanism of supercapacitive interfacial IFS, researchers have developed various

solid-solid IFS with different microstructures by combining ionic electrolytes with porous solid materials.

Generally, supercapacitive interfacial sensing can be equal to two interfacial capacitors connected in series. One is a Helmholtz layer that holds and immobilizes the majority of the counter-ions in the interfacial layer, which mainly stores energy through the physical accumulation of charges on the interface between the ionic material and the electronic conductor, instead of chemical reactions [31, 32]. The other is a pseudo interfacial layer, which is adjacent to the Helmholtz layer. It stores energy mainly through the rapid reversible redox reaction on or near the electrode surface, which changes the oxidation state of the electrode, but does not lead to phase transition [33, 34]. At present, some physical sensing models of supercapacitive interfacial sensing have been proposed, and most of them consider three physical effects, including the shape change, EDL change, and accumulated charge change. The interfacial EDL is directly proportional to the contact area of the ionic materials and the electronic conductors. In addition, the contact area is directly related to the deformation induced by the external mechanical strain [25]. Therefore, according to the classical EDL model, the black box model of supercapacitive interfacial sensing can be expressed as Equation (1).

$$C_{EDL} = \Theta(d, \varepsilon, c, T).\Lambda(p, \alpha, \beta, v_m, E_m, \eta) \quad (1)$$

where $\Theta(d, \varepsilon, c, T)$ is the capacitive value of unit contact area, which depends on many factors, including the type of electrode material, the properties of ionic electrolyte, ambient temperature and humidity, etc. [35, 36]. Hence, it is difficult to obtain an accurate estimation by this model. Usually, the capacitive value of unit contact area is often obtained through the experimental measurement in the ideal environment, which can only maintain certain accuracy. Since the capacitive value of unit contact area depends on the external environment, it needs be calibrated once again before use. Therefore, it is very important to use appropriate packaging technology to insulate supercapacitive interfacial IFS from the external environment, which can reduce the influence of the environment on the capacitive value, keep the sensing accuracy. In addition, Λ (ρ, α, v_m, E_m, β, η) is a combined parameter, which represents the contact area between the ionic materials and electrodes, where ρ represents the external mechanical force, α represents the deflection value of the ionic material, and β

represents the elastic deformation of the electrode layer. α and β can be obtained from the mechanical properties of the ionic material and the electrode layer respectively. υ_m and E_m represents the Poisson's ratio and Young's modulus of the ionic material respectively. η denotes the geometric change of the sensor. The contact area between ionic materials and electronic conductors is mainly determined by the external mechanical force and the physical properties of materials, which is less affected by the external environmental factors. Therefore, once ionic materials and the structure of IFS are determined, the contact area can be calculated precisely. According to the different kinds of ionic materials, the sensing models of supercapacitive interfacial IFS mainly include ionic liquid sensing model and solid ionic material sensing model. The ionic liquid sensing model is often used to describe the sensing process of the flexible sensor with ionic liquid as the ionic material. As shown in **Figure 2**a, the ionic liquid is directly placed between two superhydrophobic electrodes to form solid-liquid-solid IFS [7, 37]. When the external mechanical force is applied on the outer surface of the electrode, the electrode layer of the sensor is deformed, which will change the contact area between the ionic liquid and the electrode. According to the classical thin plate deflection theory, the sensing model of this structure can be expressed by Equation (2).

$$\Delta C_{EDL} = \Theta(d,\varepsilon,c,T,\varrho).(\alpha R^2 + \beta H)\frac{V_d R^2}{H^2} p \tag{2}$$

Where R and H denote the radius and height of the chamber respectively, and V_d denote the volume of the ionic liquid. The contact area between ionic liquid and electrode layer is only related to the surface area of electrode layer immersed in liquid due to the superhydrophobic electrode [38, 16]. In addition, when the electrode is deformed under pressure, and immerse in ionic liquid, the incompressible liquid drop will expand laterally due to the surface tension. Therefore, the electrode bears the main external mechanical force, and the pressure on the liquid drop is often ignored. Hence, when calculating the contact area, only the relationship between the deformation of electrode layer and the external mechanical force should be considered. Different from ionic liquid, solid ionic materials (i.e. ionic polymer matrix) are usually compressible. When IFS are subjected to external mechanical force, the electrode layer is deformed, thus squeezing the ionic polymer matrix and deforming them, as shown in Figure 2b. At this case, ionic polymer matrix bear most of the external mechanical force and

the contact area is mainly determined by the mechanical deformation of ionic polymer matrix [29, 31]. In theory, the sensing model of this structure can be derived from the original elastic contact model, which transforms the change of contact area into the elastic deformation of spherical object, and considers the Young's modulus, viscosity, friction and geometric shape of ionic polymer matrix [39, 40]. This sensing model can successfully predict the electrical response under external mechanical strain to a certain extent.

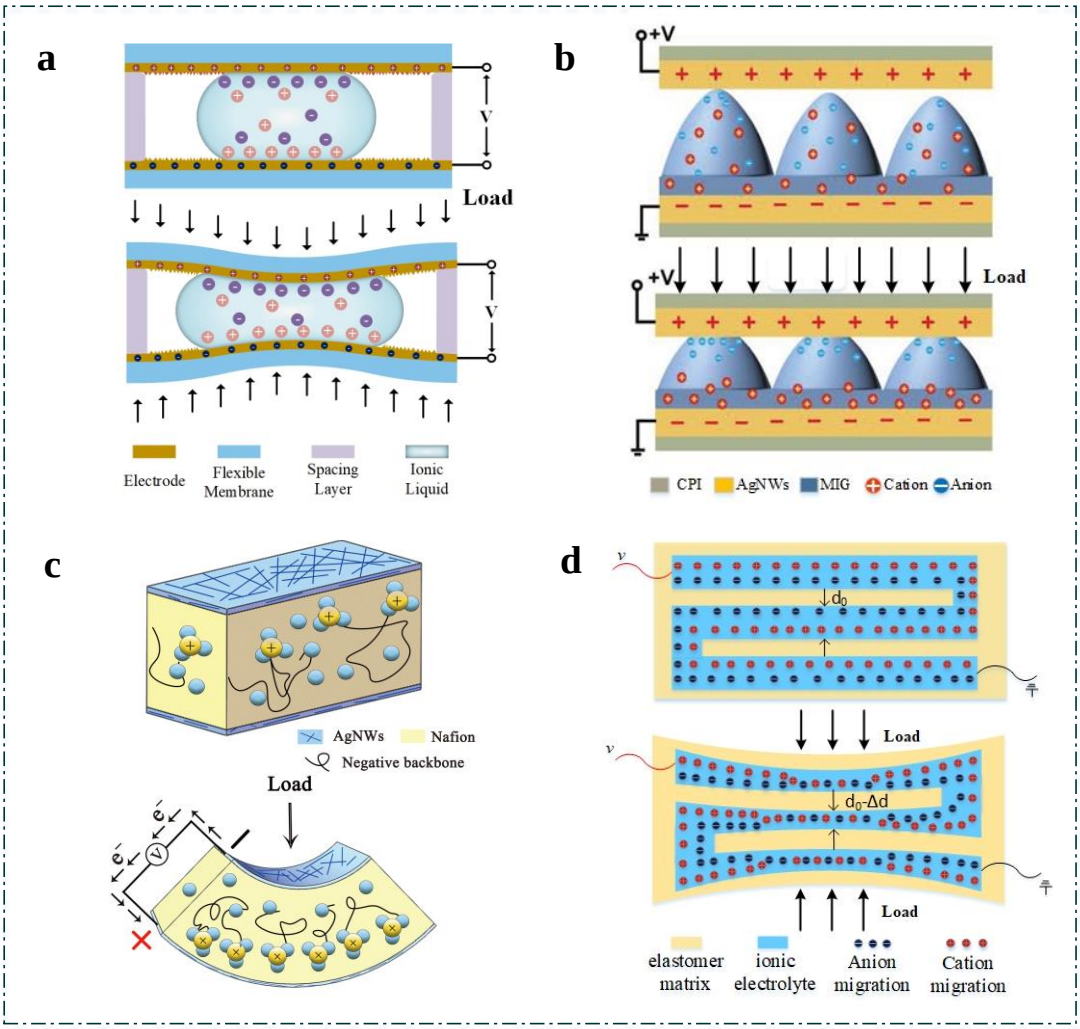

Figure 2. Typical ionic sensing structures. a) Iontronic microdroplet sensing. b) Supercapacitive interfacial sensing. Reproduced with permission.[82] Copyright 2018, Wiley-VCH. c) Piezoelectric sensing. d) Piezoresistive sensing.

2.2 Ionic piezoelectric effect

Piezoelectric IFS are made by forming noble metal electrodes on both surfaces of ionic polymer matrix as a sandwich structure, which are usually prepared by chemical or physical

methods. However, the electrochemical and mechanical properties of piezoelectric IFS prepared by physical methods are generally poor. The materials used as the electrode mainly could be noble metals, such as Au, Pt, Pd, Ag and so on [41, 42]. In addition, as the carrier of ion transport, the ionic polymer matrix plays a key role in the sensing ability of IFS, which is usually composed of polyelectrolytes. Nafion, the most used ionic polymer matrix for piezoelectric IFS, is mainly composed of perfluorinated sulfonic acid resin and solvent, in which the side-chain and main-chain of the resin constitutes the hydrophilic ion channel and the hydrophobic skeleton, respectively. Therefore, the main-chain of perfluorinated sulfonic acid resin mainly determines the mechanical properties of ionic polymer matrix, while the side-chain mainly determines the electrochemical properties [43]. In addition, the anions in the ionic polymer matrix will be attracted and fixed by the side-chains of perfluorinated polymers, while the cations combine with water molecules to form hydrated cation [44-47]. The microstructure of Nafion is shown in **Figure 3**a. According to the molecular structure, Nafion is a perfluorinated sulfonic acid ionomer membrane that has a teflon-like backbone and short side-chains terminated by sulfonic acid group, and hydrophobic fluorocarbon and hydrophilic ionic phases [48-50]. Electrolytes are also important components for ionic polymer matrix. Alkali metal ions, such as Li^+, Na^+, K^+, Rb^+ and Cs^+, are usually used as the sensing ion in electrolyte. Sometimes organic ions are also used as the sensing ion in electrolyte, such as Ca^{2+}, TBA^+, TMA^+, etc. The solvents in electrolyte are water, ethylene glycol, glycerol, propylene carbonate and ionic liquids, etc. [51, 52].

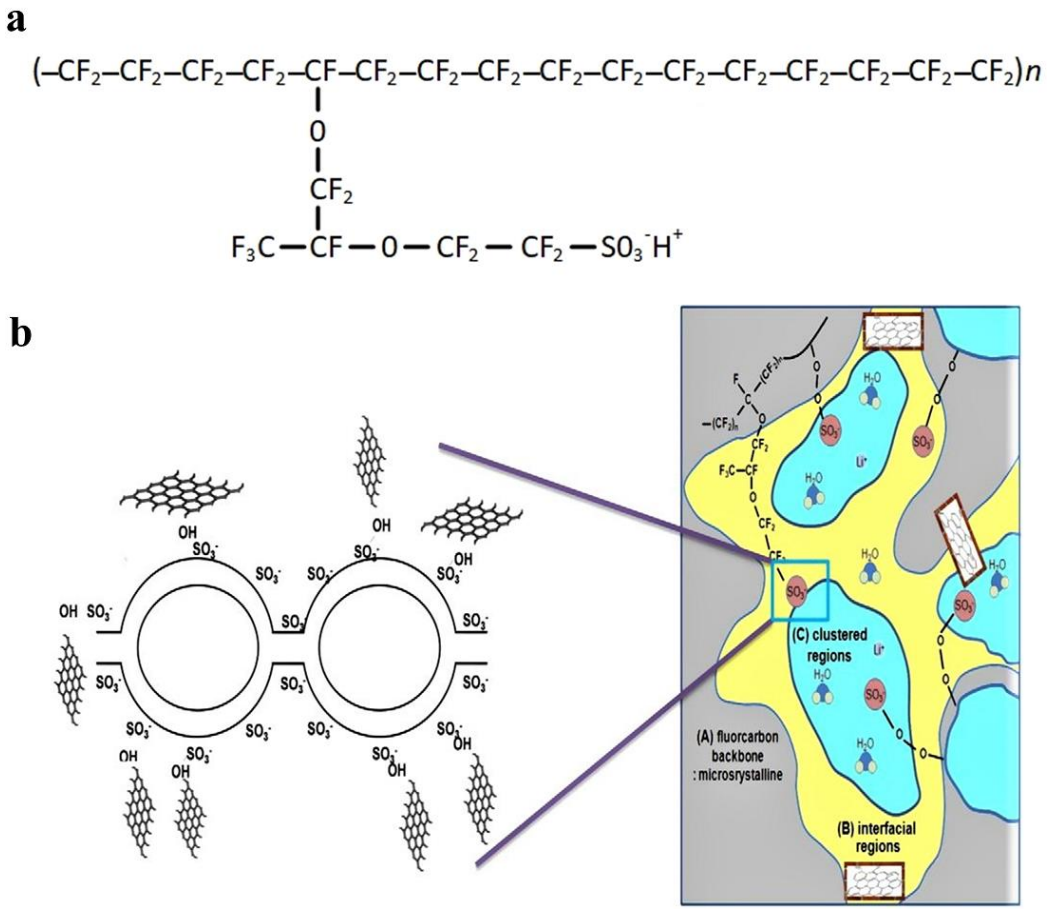

Figure 3. (a) Chemical structure of Nafion. (b) The sensing mechanism of Nafion. Reproduced with permission.[53] Copyright 2011, Elsevier.

The sensing mechanism of piezoelectric IFS involves physics, chemistry, material, and mechanics and so on, which is an extremely complex process. The current mainstream explanation shows that when Nafion absorb a certain amount of water, the hydrophilic ionic phases attracts water molecules to form spherical ion clusters [53]. Meanwhile, the ion clusters are connected by the nano-sized microchannels [54, 55], as shown in Figure 3b. When piezoelectric IFS is subjected to external mechanical strain, the hydrated cation migrates along the direction of mechanical force in the microchannel, which results in increase of hydrated cation in the stretched side and decrease of hydrated cation in the compressed side. Therefore, cations in the stretched side will increase and cations in the compressed side will decrease, thus forming a potential difference on the both sizes of piezoelectric IFS, as shown in Figure 2c. In recent years, sensing models of piezoelectric IFS have been developed [56, 57], considering three physical phenomena: the evolution of stress and strain in the sensor, ion migration and the change of electrostatic field in Nafion due to the redistribution of ions.

According to the above physical phenomena, the sensing model of piezoelectric IFS can be expressed by Equation (3).

$$\begin{cases} \dfrac{\partial C}{\partial t} + \nabla.(-D.\nabla C - zvFC\nabla\varphi - vCD_V\nabla P) = 0 \\ -\nabla^2\varphi = \dfrac{\rho}{\varepsilon} \\ \rho\ \dfrac{\partial^2 u}{\partial t^2} - \nabla.C\nabla u = F \end{cases} \tag{3}$$

Where C, φ, μ (dependent variable) denote the cation concentration, the potential in the polymer and the displacement vector respectively. D, z, v, Dv (constant) denote the cation diffusion coefficient, the charge number, the cation migration rate and the cation molar volume respectively. In addition, P, ρ (variable) represent the static pressure and the charge density in the polymer. The sensing model shows that the sensitivity of piezoelectric IFS increases with the increase of ion concentration, cation migration rate and other factors in the polymer. Therefore, it is very important to improving the sensing performance of piezoelectric IFS by increasing the ion concentration, cation migration rate, and water content in the polymer [58-60]. Besides the internal factors, the sensing performance of piezoelectric IFS is also affected by its own size. *Wang et al*. confirmed that piezoelectric IFS showed better sensing performance when the thickness of the sample increased. While the length increased, the voltage signal decreased under the condition of an equal bending. Moreover, the width has almost no influence on sensing performance [23]. Therefore, it is a feasible method to obtain stronger sensing response by increasing the thickness of the sensor and reducing the length of sensor.

2.3 Ionic piezoresistive effect

Piezoresistive IFS could perceive the resistance change when subjecting to the external mechanical strain. Compared with the classical piezoresistive sensor, piezoresistive IFS are usually composed of elastomer matrix and ionic electrolyte. As shown in Figure 2d, there are many flow channels inside the elastomer matrix filled with ionic electrolyte, and the length and cross-sectional area of the flow channel will change when external mechanical strain is applied to elastomer matrix [61, 62]. Moreover, corresponding to the holes and electrons in the

conventional electronic conductor, the cations and anions in the ionic electrolyte will migrate to the cathode and anode respectively by the presence of the electric field, thus forming the ionic fluid in the flow channel. Likewise, the cross-sectional area or length of the flow channel changes in the ionic electrolyte, which affects the impedance of piezoresistive IFS [63]. It should be noted that the elastomer matrix is the key component of piezoresistive IFS, which provide a soft and stretchable basal frame. Usually, silica gel is used as elastomer matrix with low Young's modulus, such as elastomer silicon [62], PDMS [64, 65] and Ecoflex [66]. For example, *Chossat et al.* developed a flexible sensor that can withstand 100% strain by using elastomer silicon [62], which had embedded flow channels filled with ionic electrolyte. Meanwhile, a mixture of ionic liquid and EGaln was used as ionic electrolyte, which effectively reduced the sensitivity of piezoresistive IFS to noise and further enhanced the linearity of the sensing signal. As early as 2012, *Park et al*. prepared a piezoresistive IFS by using 3D printing technology and casting technology, and they confirmed that the output signal of piezoresistive IFS was almost linear with the strain of the microchannel [67]. According to the electrolyte resistance and the relationship between the resistance and the strain, the resistance of the elastomer matrix filled with ionic electrolyte is expressed by Equation (4).

$$R = \rho \frac{L}{A} \tag{4}$$

Where ρ represents the resistivity of ionic electrolyte, and can be measured experimentally. A is the minimum cross-sectional area of the microchannel, and L is the length of the microchannel. When the resistivity of ionic electrolyte is measured experimentally, the resistance of piezoresistive IFS depends entirely on the size and cross-sectional area of the microchannel. Therefore, considering the tension and Poisson's ratio of the elastomer, the sensing model of piezoresistive IFS can be expressed by Equation (5) [66].

$$R = \frac{2L_0\rho(1+\epsilon)}{h_0(a_0+b_0)(1-v\epsilon)^2} \tag{5}$$

Where a_0, b_0, h_0 and L_0 represent the initial width of the upper bottom, the initial width of the lower bottom, the initial height and length of the flow channel, respectively, ϵ represents the tension of the elastomer, and υ represents the Poisson's ratio of the elastomer. Specifically,

because of flow channel and fluids being in the elastomer, the mechanical properties of the sensor are anisotropic, which causes the Poisson's ratio of the elastomer change. Therefore, it is difficult to keep the sensing accuracy of the model. Besides the above methods, recently, many researchers have directly prepared the piezoresistive IFS by ionic hydrogels, the resistance of which is mainly affected by the deformation. This type of piezoresistive IFS usually requires unique structural design, such as zigzag structure [68]. When subjecting to external mechanical strain, the sensor can monitor the resistivity to further obtain the strain value [69].

3. Material compositions

IFS are usually composed of the polymer matrix, electrolyte and electrode layers. The electrodes have need to be excellent conductivity to realize the conduction of sensing signals. The ionic electrolyte and polymer matrix together constitute the ionic polymer matrix. The polymer matrix usually has good compressibility and the ionic electrolyte has excellent physical and chemical properties. In this section, we will focus on the up-to-date ionic polymer and the electrode materials used to IFS. As for the ionic electrolyte, we will not discussed here and please refer to literatures 30 and 28 in detail. The material properties of the polymer matrix and the electrode, such as Young’s modulus, polarity, fracture coefficient, etc. will also be included. In addition, the emerging characteristics of materials in recent years will be presented.

3.1 Polymer matrixes

Initially, IFS usually used ionic liquids directly as the matrix. Due to good physical and chemical properties, ionic liquids have shown great potential in supercapacitive interfacial IFS. However, this kind of IFS often has some defects, such as low durability and complicated fabrication technology, which make it difficult to achieve the high sensitivity and high durability [70, 71]. To enhance the stability of IFS and improve its plasticity, *Angell et al.* mixed ionic liquid and a polymer to prepare a solid ionic polymer matrix [72]. The solid ionic polymer matrix had merged the properties of the ionic liquid and the plasticity of the solid polymer, which greatly enhanced the stretchability, mechanical adaptability, stability and

sensitivity of IFS. In addition, in the latest research, researchers have developed many new ionic polymer matrixes with novel characteristics, such as biodegradable polymer matrixes, self-healing polymer matrixes, and other matrix materials. We will also discuss them in detail in this section.

3.1.1 Polymer matrixes for supercapacitive interfacial IFS

Classical ionic polymer matrixes. Based on preparation methods, supercapacitive interfacial IFS can be categorized into two types of structures, as shown in **Figure 4**. For the first structure (Figure 4a), ionic gel is most used as a dielectric, which is sandwiched between two stretchable electrodes to form an EDL capacitor [73, 74]. For the second structure (Figure 4b), a stretchable elastomer is sandwiched between two ionic hydrogel matrixes to form two EDL capacitors in series [75, 76]. The two hydrogels connect to a capacitive meter through two metallic wires. In addition, the stretchable elastomer sandwiched between two ionic hydrogel matrixes is usually a kind of soft material, which can further enhance the compressibility of supercapacitive interfacial IFS. Meanwhile, the stretchable elastomer also plays an insulating role due to the conductivity of the hydrogel.

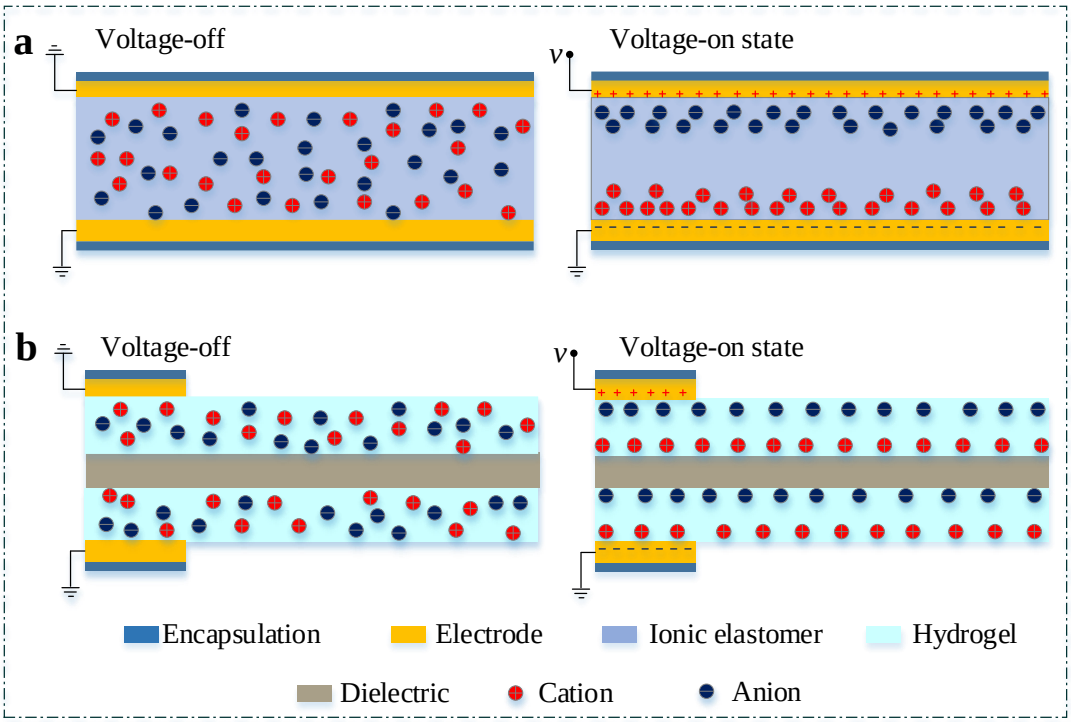

Figure 4. The typical structures of supercapacitive interfacial IFS.

From Figure 4a, the ionic polymer matrix is usually a dielectric made up of an ionic

electrolyte and gel. When the ionic gel matrix contacts with the electrode, the positively charged electrode will repel cations, while anions will be attracted to the electrode surface. On the contrary, the negatively charged electrodes will repel anions, while cations will be attracted. Therefore, the EDL is formed at the interface between the ionic gel matrix and two electrodes [77]. Specifically, this kind of gel contains a spatial network structure through the blending or crosslinking of molecular chain. The ionic electrolyte fills in these spatial network structures, and can flow freely to realize the ions migration [78, 79]. Different from hydrogel, the crosslinking degree of this kind of gel is often larger, and the network structure is more compact, which reduce the water absorption and the mobility of ions. Since the ionic electrolyte can only be fully mixed in a polar polymeric matrix with potential high ionic conductivity, the choice of polymer mainly depends on the polarity of the material. Therefore, the polymer can be a block polymer that can be chemically crosslinked, such as acrylate monomers, polyethylene glycol diacrylate (PEGDA) and hydroxyethyl methacrylate (HEMA) [80, 81], or a thermoplastic polar polymer showing high compatibility, such as poly(vinylidene fluoride)–hexafluo-ropropylene (PVDF-HFP), thermoplastic polyurethane (TPU) and poly(vinyl alcohol) (PVA) [24, 62, 82, 83]. As shown in **Figure 5**a, the researchers mixed PVDF-HFP and ionic liquid ([EMIM] [TFSI]) to prepare an ionic gel membrane with a high aspect ratio microstructure by a silicon sandpaper mold. This matrix membrane had good flexibility and stability, which can withstand more than 7000 cycles by strain. Moreover, this kind of IFS can be applied to human skin to sense human's pulse, heart rate and tactile perception [62].

From Figure 4b, two ionic hydrogel matrixes are used to form two EDL capacitors in series [84]. Because of the good conductivity of hydrogel, an elastic dielectric is used to avoid conduction between the upper and lower electrodes of supercapacitive interfacial IFS. Different from classic gels, Hydrogel is a gel with water as dispersing medium. It has a hydrophilic three-dimensional network structure, which can rapidly swell in water and retain a large volume of water without dissolution. The water absorption is closely related to the crosslinking degree of hydrogel. As the crosslinking degree decreases, the water absorption of hydrogel will increase, even reaching 99%. The three-dimensional network of hydrogel has a mesh size of ~10 nm, which is much larger than the size of a water molecule, allowing water

molecules in the hydrogel to maintain the same chemical and physical properties as in liquid water. Dissolving salt in the hydrogel, which change the resistivity of the hydrogel from ~18.2MΩm to ~10^{-1}Ωm, depending on the type and concentration of the salt [6]. When applying a voltage, the ion current will form inside the hydrogel, which will make the hydrogel become a conductor. In addition, the resistance of the hydrogel changes with the stretch length, and follow a square-law relationship (that is, the change in resistance is proportional to λ^2, and λ means stretch ratio) [85]. Compared with classic gels, hydrogel has better stretchability and biocompatibility, which can work more several times than the initial length. Therefore, it has great advantages in many fields, such as artificial skin [86, 87], artificial axons, ion-electronic liquid crystal devices, touch panels, etc. [88-90]. *Yoon et al.* shows a type of IFS with ionic hydrogel membranes, in which the carbon nanotube/polydimethylsiloxane composites was used as the matrix and [EMIM] [TFSI] was used as the ionic electrolyte [91]. This kind of IFS with the sensitivity of 9.55 kPa^{-1} and ultra-low response limit of less than 5Pa can be used to monitor muscle movement, respiratory and arterial pulse waveform in real time, showing good biocompatibility. In addition, *Sun et al*. used sodium chloride electrolyte and acrylamide to prepare IFS with highly sensitive hydrogel, and attached VHB to the surface of the sensor to isolate the external environment. There is a broad dynamic range under the external stimuli for this sensor. Even under the pressure of less than 1 kPa, it still had a very high sensitivity [92]. However, the water molecules in the hydrogel are very volatile, it is usually necessary to package a layer of elastomer on the outer surface of IFS for electrical insulation and against water loss, such as PDMS, VHB, etc.

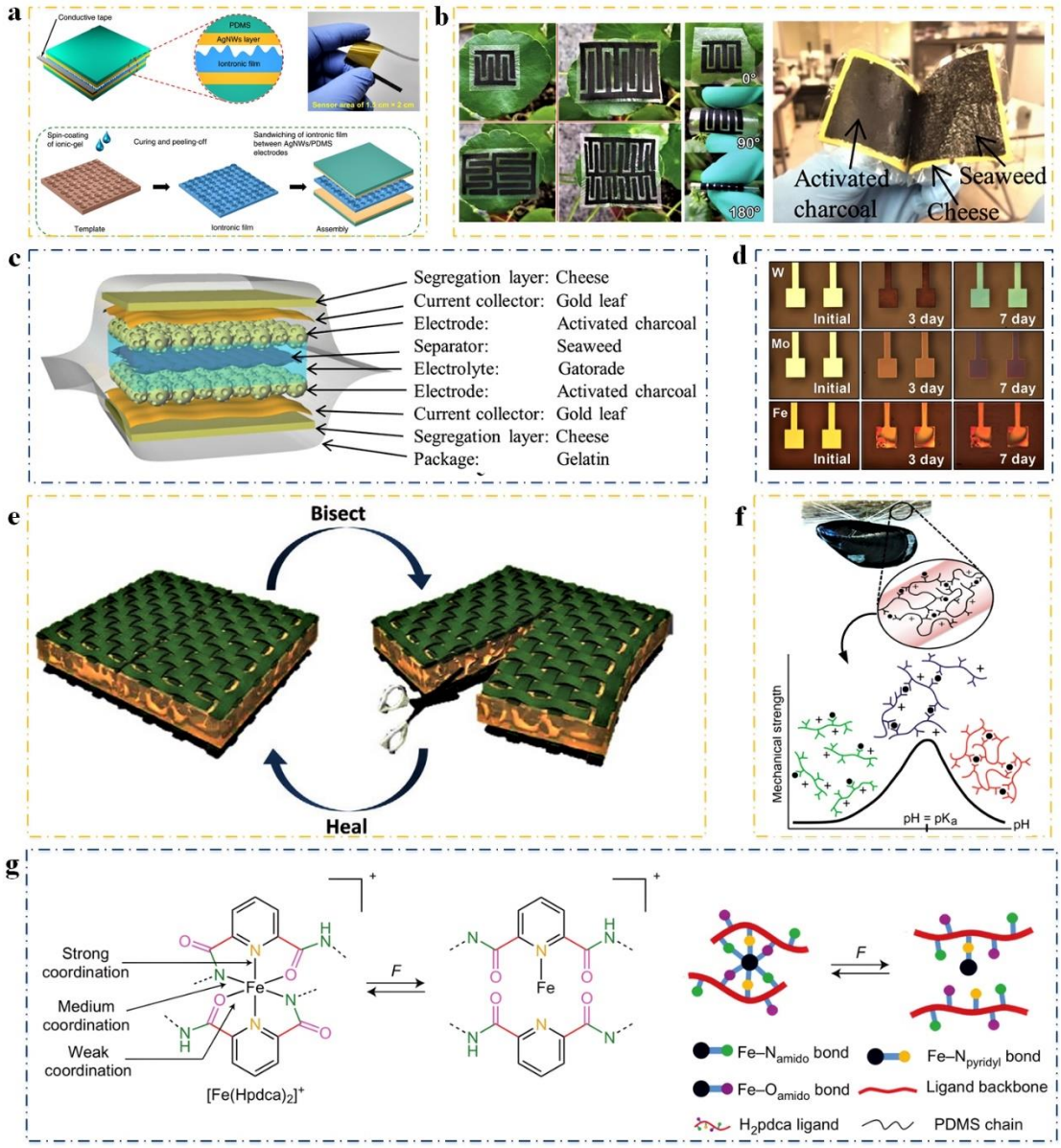

Figure 5. a) Ionic gel membrane with a high aspect ratio microstructure was prepared by a silicon sandpaper mold. Reproduced with permission.[62] Copyright 2018, American Chemical Society. b) IFS with renewable mesoporous cellulose membrane. Reproduced with permission.[102] Copyright 2017, Wiley-VCH. c) Edible supercapacitive interfacial IFS. Reproduced with permission.[106] Copyright 2016, Wiley-VCH. d) Biodegradable IFS. Reproduced with permission.[110] Copyright 2017, Wiley-VCH. e) IFS based on self-repairing hydrogel. Reproduced with permission.[121] Copyright 2019, Elsevier. f) Self-healing mussel-inspired multi-pH-responsive hydrogels. Reproduced with permission.[122] Copyright 2013, American Chemical Society. g) Crosslinking complexes by mixing strong ligands and weak ligands. Reproduced with permission.[126] Copyright 2016, Macmillan.

Biodegradable polymer matrixes. Biodegradable polymer matrix is usually composed of organic materials, which can be decomposed by microorganisms or organisms, such as enzymatic reactions of microorganisms or hydrolysis reactions in a non-enzymatic environment. The specific mechanisms of biodegradation can be different depending on the materials, and they can be digested by many animals and microorganisms, and even dissolved in water. In recent years, a few well-known biodegradable materials have been developed, such as agarose [93], cellulose acetate [94], and chitosan [95]. Among them, cellulose with the special crystal shape, surface structure is one of the oldest biodegradable materials, which is frequently used as a matrix or modified matrix for flexible electronic equipment [96-98]. Meanwhile, because of its convenience, low cost, easy degradability and environmental friendliness, it has been used as biodegradable matrixes in many studies [99, 100]. For example, *Zhang et al*. used nano-cellulose-derived hierarchical porous carbon (HPC) as the ionic polymer matrix to prepare supercapacitive interfacial IFS with excellent electrochemical performance, and the capacitive value of which reached 10.84 F cm^{-3} under a load of 0.25 A g^{-1} [101]. Nano-cellulosic carbon, composed of interconnected nanofibers, has a three-dimensional porous structure, nanofibers of which have an ultra-high surface area (2046 $m^2.g^{-1}$). These properties help ionic electrolytes migrate quickly. Moreover, nano-cellulose carbon has good reproducibility and biodegradability, and can be used in bio-friendly ionic sensors. For example, *Zhao et al*. prepared a flexible, transparent, and renewable mesoporous cellulose membrane through a simple and scalable liquid-solid phase inversion method (Figure 5b). This matrix membrane had a uniform porous of about 24.7 nm and an ultra-high porosity of 71.18% [102]. The activated carbon and potassium hydroxide were used as the electrodes and the ionic electrolyte, respectively. Experimental results showed that this IFS exhibited a high areal capacitance of 153.34 mF·cm^{-2} at 10 mV s^{-1} as well as high flexibility without any performance degradation when bent in 180°. In addition, this kind of IFS had a service life of 10,000 cycles and a capacitance retention rate of 84.7%. Although the cellulose-based matrix has good sensing sensitivity and biodegradability, the prepared supercapacitive interfacial IFS lacks stretchability due to the tight entanglement of the cellulose molecular structure, which severely limits the applications of the sensor.

Although cellulose-based biodegradable matrix has good biodegradability, they often

need to use some organic solvents, acid-base solvents, or other hazardous substances when preparing them. The cellulose-based matrix cannot be directly digested and absorbed by the human body, and cannot be used as an implantable electronic device [103, 104]. To solve this problem, some researchers have used edible materials to prepare IFS [105]. As shown in Figure 5c, *Wang et al*. used cheese and seaweed as the polymer matrix, and used edible activated carbon and egg white as electrodes to prepare edible supercapacitive interfacial IFS [106]. This sensor exhibited an excellent capacitive value of 78.8 F g^{-1} under 1A g^{-1}. In addition, this sensor had a service life of 1000 cycles and a capacitance retention rate of 92.3%. Besides cheese and seaweed, *Hu et al*. mixed flour and edible activated carbon to prepare essentially self-healing, biodegradable stacked supercapacitive interfacial IFS, which can be rapidly degraded in gastric juice [107]. Although the edible matrix shows stretchability and harmlessness, its mechanical strength is low and its stability is poor, which brings difficulties to practical application. Meanwhile, the hydrolyzed matrix has also been developed, such as silk, poly (1,8-octanediol-cocitrate) (POC), PVA, and poly(lactic-co-glycolic acid) (PLGA), etc. [108, 109]. *Lee et al*. used water-soluble metal electrodes, PLGA-based matrix and hydrogel electrolyte (agarose gel) to prepare a hydrolyzed miniature supercapacitive interfacial IFS [110]. This sensor showed stable operation for 6 hours in PBS at 37°C, and then degraded after 7 hours (Figure 5d). It is particularly surprising that during repeated charge/discharge cycles, electrochemical corrosion will produce a metal oxide coating, which promoted the formation of pseudocapacitance phenomenon at the interface between the water-soluble metal electrode and the matrix. As a result, the sensing signal was significantly enhanced, which made the sensor still having a very high sensitivity after many cycles. However, the use and storage of hydrolyzed matrix are greatly affected by environmental factors, especially environmental humidity, so a good packaging strategy is very necessary.

Self-healing polymer matrixes. IFS will be damaged when they are overly stretched or bent. Therefore, self-healing is an important function for IFS to prolong its service life, and reduce production costs. According to different self-healing methods, self-healing matrixes can be categorized into two types, namely external self-healing matrix and internal self-healing matrix. The external self-healing matrix needs to use external conditions to achieve the self-healing, such as energy (heat or light) [111, 112], catalyst [113], solvent [114] or

plasticizer [115], etc., which severely limits the use of external self-healing matrix. *White et al*. injected capsules and catalysts into the polymer matrix. When the polymer matrix was damaged, the damaged capsules would release the reagents to fill and repair the damaged surface under the action of the catalyst [116]. However, because the repair process will consume the capsules in the polymer matrix, this self-healing ability is limited, which makes this material undesirable when used as a self-healing matrix for IFS.

The inside of internal self-healing matrix usually has dynamic cross-linking chemical bonds, which can reestablish intermolecular bonds in the polymer matrix, so that the damaged surface can be repaired [117]. Such chemical bonds are usually non-covalent bonds [118, 119], such as hydrogen bonds, disulfide bonds, coordination bonds [120], etc. For example, because dopamine and Fe(III) can easily form new coordination bonds, the researchers mixed dopamine and amine functionalized polymers to prepare a self-repairing hydrogel [121-123] (Figure 5e). Specifically, the strength of coordination bonds between dopamine and Fe(III) depends on the PH level. When the PH level increases from acidic to alkaline, the hydrogel will heal quickly. Therefore, the self-healing speed of the hydrogel can be controlled by the PH level (Figure 5f). In addition, supramolecular gel based on peptide/amino acid is also an important field of current research about internal self-healing matrix. Such supramolecular gels can form metallo-gels with various transition metals, including cholesterol derivatives, pyridine complexes, and various metal organic frameworks and so on. Due to the presence of transition metals, metal ions in the supramolecular gel are held near the ligand through strong interaction, which allows the coordination bond to be reformed [124]. *Basak et al*. developed a series of multi-stimuli responsive self-healing metallo-hydrogels with peptide/amino acid [125]. This type of hydrogel exhibited responsiveness to heat, mechanical vibration, PH level and external chemicals. It is worth noting that the self-healing property and the stiffness of these metallo-hydrogels can be tuned by varying the chain length of the corresponding gelator amphiphile. However, polymer matrix that relies on weak bonds for self-healing often cannot provide sufficient mechanical strength. The combination of strong ligands and weak ligands can not only achieve self-healing functions, but also have excellent extensibility. For example, *Li et al*. prepared crosslinking complexes by mixing strong ligands and weak ligands. These crosslinking complexes consist of 2, 6-pyridinedicarboxamide ligands, which coordinate to Fe

(III) centres through three different interactions, including a strong pyridyl–iron one, and two weaker carboxamido–iron ones through both the nitrogen and oxygen atoms of the carboxamide groups. As a result, the iron–ligand bonds can readily break and re-form, while the iron centres still remain attached to the ligands through the stronger interaction with the pyridyl ring, which enables reversible unfolding and refolding of the chains [126], as shown in Figure 5g. Experiments showed that the IFS prepared by this method can be stretched to 45±2 times of its original length and recover when the strain is released. Even in the absence of any external conditions, such as plasticizers or solvents, or external energy, this matrix still showed excellent self-healing performance at a low temperature of 20℃.

Other polymer matrixes. In daily life, many materials can also be used as the matrix of ionic sensors, such as paper [127, 128], and fabric [35, 129] and so on, because of their similar structure to macromolecular polymer or large amount of ions in them. The plant material is a 3D cell wall network which plays like a compressible metamaterial that elastically collapses upon pressing plus some specific surface structures, and thus the device can sensitively respond to pressure. *Wan et al*. have directly used plant materials including flowers and leaves as the dielectric material in supercapacitive interfacial IFS [130]. The device works over a broad-pressure range from 0.6 Pa to 115 kPa with a maximum sensitivity of 1.54 kPa^{-1}, and shows high stability over 5000 cyclic pressings or bends, as shown in **Figure 6**a. Moreover, Paper is composed of cellulose with unique porous structures and has natural hydrophilicity. The cellulose can absorb water molecules through the capillaries and diffuses into the interior. In addition, because cellulose can be functionalized, paper can be modified by adding some functional additives, such as carbon-derived materials, conducting polymers, and metal nanocomposites, to produce unique sensing properties. For example, *Tao et al*. mixed paper with graphene oxide solution to obtain graphene oxide paper [131]. Experiments showed that the performance of IFS based on thin paper has been greatly improved, and the value of sensitivity is as high as 17.2 kPa^{-1} during the pressure range of 0-20 kPa. In addition, *Gong et al*. prepared IFS with high sensitivity and flexibility by sandwiching thin paper impregnated with ultra-thin gold nanowires between two sheets of thin polydimethylsiloxane [132]. This IFS can work at the voltage of 1.5V, which had low energy consumption (<30μW) and can sense pressures as low as 13 Pa. Meanwhile, This IFS had a fast response time (<17 ms), high

sensitivity (>1.14 kPa^{-1}) and excellent stability (>50,000 load-unload cycles). Although recent research has successfully demonstrated the advantages of paper-based matrix such as high sensitivity, low cost, and simple process, other unique advantages of paper have not been fully demonstrated, such as printability, cutability, and foldability. As shown in Figure 6c, *Li et al*. printed ionic electrolyte and conducting patterns on paper to prepare ionic sensing paper, which can be cut at will and used as a flexible sensor [36]. This method makes full use of the unique advantages of paper, such as printability, cutability and foldability, and provides conditions for large-scale production. Although paper-based matrix has made great progress, the use of paper for IFS is still in its infancy. The same as the structure of paper, the inside of the fabric also has a unique porous structure, which can also be used as the polymer matrix for IFS, as shown in Figure 6b. Thanks to its softness, deformability and durability, many fabric-based ionic sensing devices have been realized, such as monitoring temperature and cerebral oximetry by attaching stretchable polyimide electrodes onto a textile substrate [133], sensing both cardiac and respiratory signals using a piezoelectric film attached onto conducting fabrics [134], blending conducting fibers in textile to assess body movements or gesture detections by strain levels [135, 136] and so on.

The skin of animals and humans is rich in ionic electrolytes and is also one of the natural ionic polymer matrixes. As shown in Figure 6d, *Zhu et al.* successfully fabricated an epidermal ionic pressure sensor that perfectly fitted human skin by using human skin as the signal interface of IFS [127]. This sensor used human skin as driving voltage to achieve high pressure sensitivity and high signal-to-noise ratio, which can sense ultra-low amplitude fluctuations of the body and the stimulation of external mechanical strain. In addition, the ability to monitor various vital signals of human body, such as blood pressure waveform, respiratory waveform, muscle contraction, and tactile perception, has been verified as well. Therefore, it has broad prospects in emerging wearable applications. In general, IFS using human skin as the signal interface simplifies the device structure and reduces related manufacturing complexity. Meanwhile, it can be attached to the human body to provide safer and more comfortable solutions for long-term wearable applications.

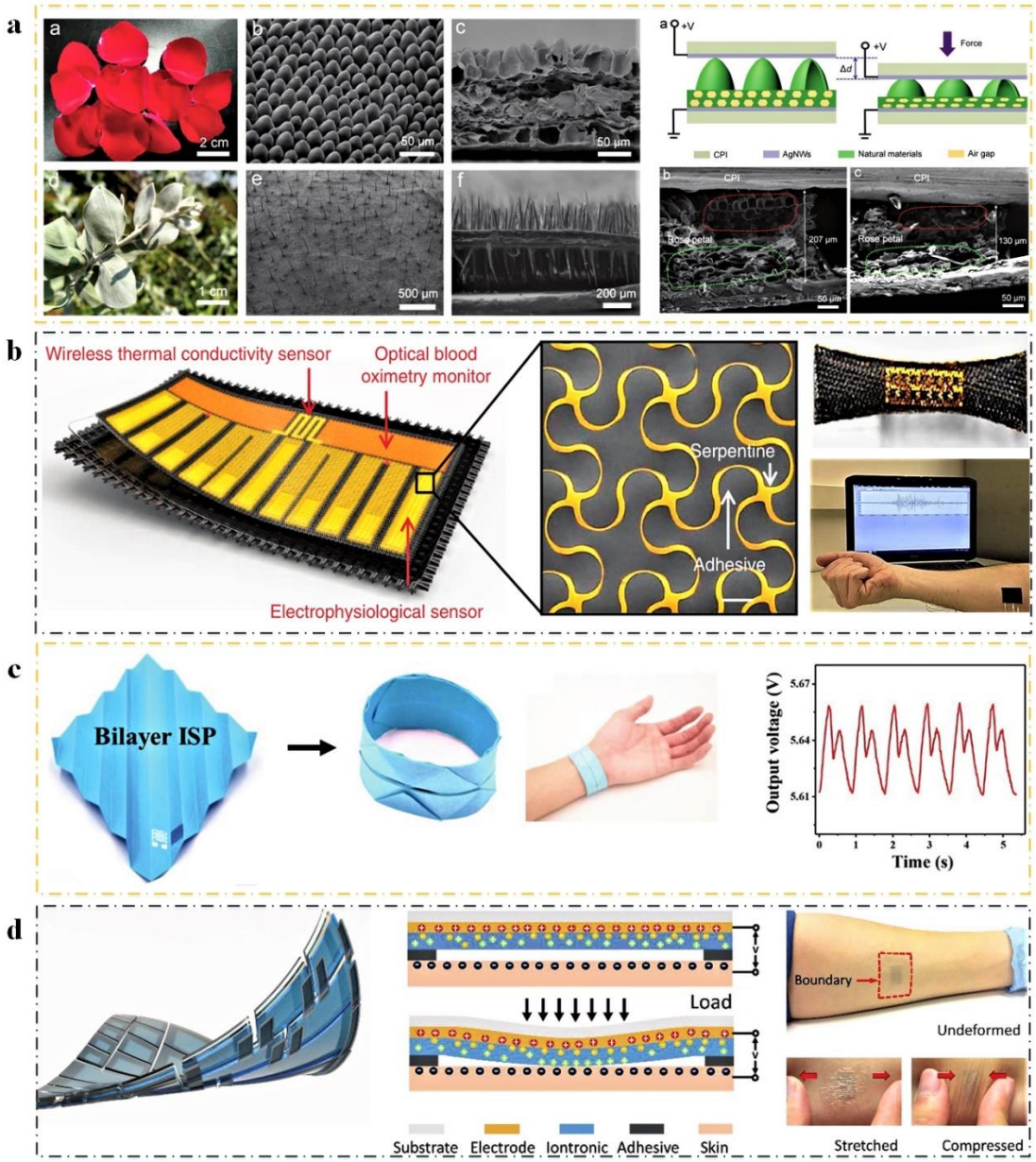

Figure 6. Self-healing matrixes and other materials. a) IFS based on plant materials. Reproduced with permission.[130] Copyright 2018, Wiley-VCH. b) Fabric-based ionic sensing devices. Reproduced with permission.[133] Copyright 2014, Macmillan. c) IFS with unique advantages of paper. Reproduced with permission.[36] Copyright 2019, Wiley-VCH. d) IFS that perfectly fits human skin by using human skin as the signal interface. Reproduced with permission.[127] Copyright 2018, Wiley-VCH.

3.1.2 Polymer matrixes for piezoelectric IFS

The ionic polymer matrixes used in piezoelectric IFS are usually made up of polyelectrolytes，which can be categorized into commercial polymer matrix and customized

polymer matrix. Currently, commercial polymer matrixes include Nafion (perfluorinated polymers) produced by Dupont Company, Flemion produced by Asabi Class Company, and Aciplex produced by Asabi Chemical Company. Customized polymer matrixes include recast commercial polymer matrix, doped polymer matrix and synthetic polymer matrix [137]. Macroscopically, the ion concentration and diffusivity of the polymer matrix have an important influence on sensing performance of piezoelectric IFS. Therefore, improving the existing polymer matrixes have always been one of the research hotspots for piezoelectric IFS. At present, the most used polymer matrixes is Nafion. Nafion ionic matrixes can be obtained by solution casting method, which is greatly beneficial to the direct modification of Nafion ionic matrixes [138-140]. *Kim et al*. firstly proposed to obtain Nafion matrixes with different thicknesses by the casting process, and prepared Nafion ionic matrixes ranging from millimeters to centimeters [141]. In addition, *Sang et al*. obtained Nafion ionic matrixes with different thicknesses by the heating and pressure-bonding process [142]. Except for increasing the thickness of the polymer matrix, an improved Nafion ionic matrix can also be obtained by doping functional particles in the Nafion solution and casting process [143, 144]. For example, *Nguyen* [145] *et al*. mixed Nafion and surface-modified fumed silica, which improved the ion concentration and water retention of the ionic polymer matrix. *Lee* [146] *and Zhang* [147] *et al*. improved the ion diffusivity of Nafion ionic matrix by doping carbon nanotubes (CNT). *Khan* and *Jung* improved the elastic modulus of the polymer matrix by doping graphite and fullerene [148, 149]. There are still many doping studies based on Nafion ionic matrix, but the results are not always able to improve the sensing performance due to the limitations of doping process. Doping process improves the sensing performance of ionic sensors by improving the ion concentration and diffusivity of ionic polymer matrix. However, there is no relevant theoretical investigation from these two aspects, which need to be further clarified.

Besides polymer matrix obtained by casting and doping technology, developing novel ionic polymer matrix is also an important research direction for the improvement of piezoelectric IFS [150-152]. Some researchers in Korean institutions have made outstanding progress in this field. *Il-Kwon et al*. have successively developed SSEBS, SPSE, SPEI, PSMI-PVDF copolymers and SPEEK-PVDF copolymer ionic matrixes [153]. *Jeong et al*. developed a new matrix material by synthesizing a series of fluorinated acrylic ionic polymers

[154]. *Jang Yeol Lee* developed new matrix materials such as PVDF-co-HFP, PE-co-TFE, and PTFE-co-HFP through radiation grafting [155]. Besides the above materials, some new materials with excellent performance can also be got through blending or crosslinking. For example, PVA can be a crosslinker for sulfonated polymer due to lots of OHs existing in its main chain, such as with PVA and poly (styrene sulfonic acid-co-maleic acid) (PSSA-MA) compounds. Recently, *Wang et al.* [156] synthesized a crosslinked PVA/SPTES ionic exchangeable matrix with direct copolymerization and post-heating method, as shown in **Figure 7**a. At 120°C for 1h, the hydrophilic (OH) and (SO_3H) groups were changed into the less hydrophilic (OSO_2) sulfonic ester groups during the dehydration (Figure 7b). The crosslinking bonding of PVA and SPTES molecules not only causes the whole matrix to be less swelling, but also alters the hydrophilic–hydrophobic balance inside the matrixes. Overall, researchers have carried out tremendous research on the new type of ionic polymer matrixes, but the sensing performances of piezoelectric IFS based on new types of ionic polymer matrixes was not able to significantly exceed those based on Nafion. It is because the research on developing new ionic polymer matrixes with the goal of comprehensively improving various parameters of electrical performance is challenging. Meanwhile, the influencing factors of the sensing performance are multifaceted and extremely complex. Therefore, the development of new ionic polymer matrix to improve the sensing performance of piezoelectric IFS has not made substantial progress.

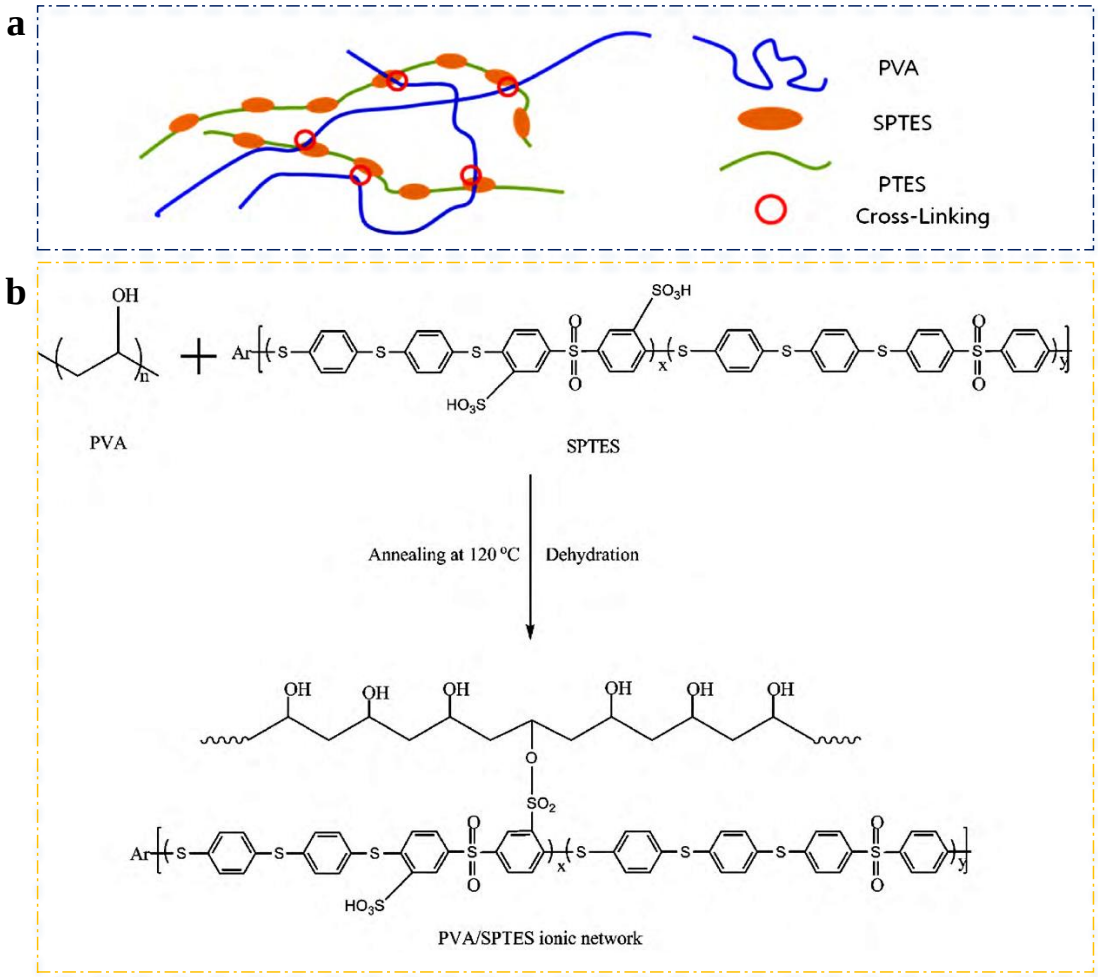

Figure 7. a) Chemical structure of PVA/SPTES. b) Crosslinking mechanism of PVA/SPTES. Reproduced with permission.[156] Copyright 2010, Elsevier.

3.2 Electrodes

Generally, two strategies can be used to prepare the stretchable electrodes of IFS. The first one is that flexible conducting materials are used to fabricate stretchable electrodes on ionic polymer matrix. Among them, more attentions are paid to the physical and chemical properties of the flexible conducting materials and the preparation process [157]. The second strategy is to adapt the deformation of IFS by the spatial hierarchical structure, in which the material properties and the formation method of the spatial hierarchical structure are the research directions, mainly including fold structure [158], wave-like structure [159], kirigami pattern [160]and so on. The performance of the electrode prepared by the first strategy mainly depends on the properties of the electrode material, including high conductivity, excellent

flexibility, low cost, and good stretchability [161]. Recently, several high-performance conducting materials have been developed, including carbon nanotubes [162, 163], graphene [164, 165], metal nanowires [166-168], percolating networks of NWs [169-172], conducting polymers [173] and conducting composites [174-177], etc. Compared with conventional metal electrodes, these conducting materials have excellent flexibility and stretchability, and many conducting materials are soluble or dispersed in various solvents, which provides preparation conditions for stretchable electrodes by some classic preparation methods，including coating techniques, printing techniques, template-assisted assembly techniques, vacuum filtration techniques, gelating techniques and electrospinning techniques [178-180]。

3.2.1 Metal-based electrodes

Electrodes formed by metal-based nanomaterials generally have good stability and conductivity. These metal-based materials can be deposited or printed on the surface of ionic polymer matrix using a micro/nano manufacturing process, which generally include 0D metal nanoparticles, 1D metal nanowires, and 2D metal percolating networks. For example, silver nanoparticles can be physically deposited on the surface of ionic polymer matrix and form a dense permeable electrode [181]. However, it is difficult to overlap among individual nanoparticles, so the kind of electrode has poor flexibility and stretchability. Therefore, many researchers investigated metal-based nanomaterials with different shapes and sizes to achieve better performances. For example, metal nanowires were considered to be ideal materials for stretchable electrodes [182]. Compared with metal nanosheets or metal nanoparticles, metal nanowires have better overlapping performance, which can maintain a good conductivity within a certain strain range. *Gao et al.* optimized the overlapping performance by preparing ultra-long silver nanowires [183]. The long silver nanowires were obtained by a continuous multi-step growth method based on silver nitrate and polyvinylpyrrolidone in ethylene glycol solution. Compared with short silver nanowires, long silver nanowires have a more effective percolating network and a lower density. Therefore, this type of electrodes achieves a high stretchability greater than 460%, as shown in **Figure 8**a. However, electrodes made of metal-based nanowires cannot maintain a relatively low sheet resistance under tensile strain. This is due to the fact that the wire-to-wire overlapping will be broken when being overly

stretched, which cause the sheet resistance increasing greatly from several Ω/sq to tens of Ω/sq. Recently, many researchers have also researched electrodes based on metal-based nanomeshes [184, 185]. For example, *Guo et al*. fabricated highly stretchable and transparent Au nanomesh electrodes on elastomers made by grain boundary lithography. The sheet resistance of these electrodes had changed from 21Ω per square to 67Ω per square under 160% strain, or after 1,000 cycles at a strain of 50%. *Cui et al.* prepared an interconnected metal-based nanomeshes based on the nanogroove as well. This electrode completely eliminated the problem of high sheet resistance and shows the stretchability of up to 50%, as well as good conductivity and optical transparency [186]. In addition to preparing metal-based nanomeshes by grain boundary lithography or nanogroove, researchers also tried to weld metal-based nanowires to form completely interconnected metal-based nanomeshes by sintering or electroplating process. For example, *Su et al*. used high intensity pulsed light (HIPL) equipment to sinter the copper nanowires spin-coated on the flexible polymer matrix. The copper nanowires were welded to each other to form completely interconnected nanomeshes, which improved the conductivity and stability of the electrode. In addition, the strong light emitted by the HIPL equipment effectively removes the oxides and hydroxides on the surface of the copper nanowires, and make the copper nanomeshes maintain excellent performance for a long time [187]. Moreover, *Liu et al*. prepared the silver nanomeshes sprayed on the flexible polymer matrix by capillary-force-induced cold welding process. Experiments showed that the nanoscale, capillary force is a powerful driving force that can effectively cause self-limited cold welding of the wire–wire junction for AgNWs. The capillary-force-induced welding can be simply achieved by applying moisture on the AgNWs film, without any technical support like the addition of materials or the use of specific facilities. The flexible stretchable electrodes prepared by this method can still maintain high electrical conductivity after 5000 bending cycles [188], as shown in Figure 8b.

Liquid metals (such as gallium indium alloys, eutectic gallium indium alloys) are widely used in flexible electronic devices due to their high conductivity, good electrical stability, and high surface tension. Recently, a liquid metal electrode with good optical transparency and stretchability has been prepared by laser-based microfabrication technique, which has a low sheet resistance of 2.95Ω/sq and a strain limit more than 100% [189]. Benefiting from the good

conductivity and fluid properties of liquid metal, *Wang et al.* prepared a highly stretchable electrode by masked liquid alloy printing, which showed a good stability under the 10,000 times cyclic tensile deformation [190] (Figure 8c). However, the liquid metal electrode has some defects such as low chemical stability [191] and complex preparation process, which severely limits its application for IFS. Besides the direct use of metal-based materials to prepare stretchable electrodes, in recent studies, many researchers have mixed metal-based nanomaterials and polymers to form conducting inks, and used various simple preparation processes to generate stretchable electrodes, such as electrospinning, inkjet printing and spin coating. For example, *Shin et al*. used spin coating process to prepare flexible electrodes by mixing gold nanomaterials, polyelectrolyte gels and nanofibers, which can still maintain excellent conductivity even more than 1500 tensile cycles [192], as shown in Figure 8d. In addition, *Song et al*. designed a simple strategy to directly print highly conducting and stretchable flexible electrodes [193]. In this method, the metal precursor solution is printed on the matrix by an inkjet printing technology, and a large number of metal nanoparticles are generated on the surface of flexible polymer matrix by a chemical reduction method. This strategy can easily form flexible electrodes on the surface of various complex structures, which provides alternative for the preparation of IFS with complex 3D structures.

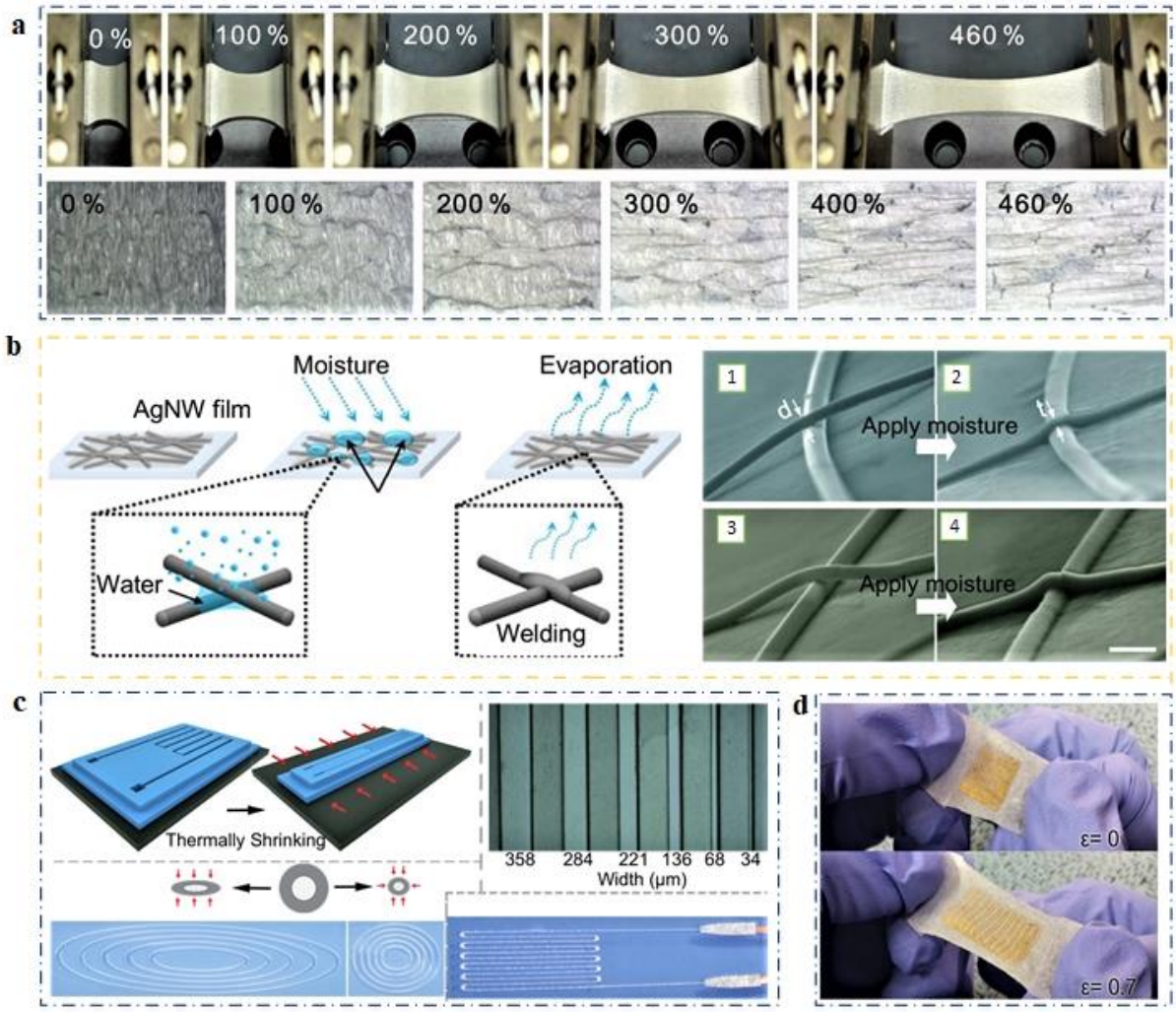

Figure 8. Metal-based electrodes. a) electrode based on long silver nanowires. Reproduced with permission.[183] Copyright 2012, Wiley-VCH. b) Silver nanomeshes by capillary-force-induced cold welding process. Reproduced with permission.[188] Copyright 2017, American Chemical Society. c) Liquid metals electrode by masked liquid alloy printing. Reproduced with permission.[190] Copyright 2018, American Chemical Society. d) Flexible electrodes by mixing gold nanomaterials, polyelectrolyte gels and nanofibers. Reproduced with permission.[192] Copyright 2014, Wiley-VCH.

3.2.2 Non-metal-based electrodes

Although metal-based materials have good conductivity, there is still the challenge of poor stretchability for practical applications. Recently, researchers have developed several non-metal-based materials as the electrode of IFS with good stretchability, including carbon nanotubes, graphene, conducting polymers, etc. Carbon nanotubes were firstly used in flexible

electrodes in 2004, and since then they have been widely used in flexible energy storage devices [194, 195] and flexible sensors [196, 197]. However, carbon nanotubes have some drawbacks, such as high sheet resistance and low stretchability, which severely limit their practical applications in flexible electronics. Recently, some researchers have discovered that by arranging carbon nanotubes in particular directions, the conductivity and stretchability of carbon nanotube electrodes can be effectively improved. As shown in **Figure 9**a, a solution-free self-dispersion process was used to prepare carbon nanotube electrodes with vertical and parallel arrangement. During the stretching process of the electrode, the vertical arrangement in the carbon nanotube array would be transformed into a horizontal arrangement to form an overlapping layer, which could withstand a strain of 35%, had a transmittance of 83.4% and a sheet resistance of 24Ω/sq [198]. However, the deformability of carbon nanotube electrode seriously depends on the direction of the carbon nanotube. *Liu et al*. cross-stacked carbon nanotube layers on a square frame to prepare the flexible electrodes, in which the direction of first layer is perpendicular to the second layer [199]. This carbon nanotube electrode was isotropic in conductivity, but the mechanical properties depend on the stretching direction. In order to further improve the stretchability of carbon nanotube electrodes, wavy carbon nanotube electrodes have been developed, which are usually prepared on the pre-stretched polymer matrix. When the polymer matrix is restored, the carbon nanotube electrode will form a wave shape. For example, *Zhang et al*. prepared a carbon nanotube flexible electrode on a 50% pre-stretched polymer matrix, which can withstand a strain limit more than 50% [200]. Meanwhile, to further improve the conductivity of carbon nanotube electrodes, it is also an effective method to combine carbon nanotubes with conducting metals. As shown in Figure 9b, *Xu et al.* transferred the carbon nanotube electrode with gold/palladium metal to a pre-stretched flexible matrix to prepare a wavy carbon nanotube electrode. The electrode has a sheet resistance as low as 72Ω/sq with an excellent stretchability. When the tensile strain reaches 100%, the sheet resistance only increases by 4.1% [201].

Since being firstly proposed in 2004, graphene has a huge application potential in IFS due to good mechanical flexibility and chemical stability [202]. Ideally, carrier mobility of graphene is as high as 200,000 $cm^2 \cdot V^{-1} \cdot s^{-1}$, which is higher than carbon nanotubes. Its resistivity is about $10^{-8}\Omega \cdot m$, which is below most metals including silver and copper. However, actually, graphene

generally contains many grain boundaries and defects, which make its conductivity much lower than the theoretical value. During the stretching process, the original graphene electrode produces a large amount of cracks, which will result in a sharp decline in conductivity. Because graphene itself cannot be stretched as much as polymer, the graphene electrode needs to be modified by other materials or structural optimization to achieve the good stretchability. For example, the graphene electrode can withstand a strain of up to 120% by adding nano molecular bridges [203]. Moreover, a buckled structure or non-coplanar serpentine structure can be used to enhance the deformability of graphene, as shown in Figure 9c. The preparation method of buckling structure or non-coplanar serpentine structure is the same as that of the wavy carbon nanotube electrodes. In addition to the stretch/release preparation process, a graphene electrode with a particular structure can also be grown by chemical vapor deposition on a patterned copper foil [164, 204], which has good conductivity and retractability. However, these advantages have been offset by complex manufacturing processes, high cost and low yield.

The conducting polymer achieves the abilities of high electrical conductivity by electron flow or ion migration. Because of its good mechanical properties and electrical conductivity, it is considered to be a very promising electrode material in IFS. There are many kinds of conductive polymers, including polyacetylene, polythiophene, polypyrrole, polyphenylene, polyaniline, and PEDOT [205-207]. In particular, poly (3, 4-ethylene dioxythiophene) polystyrene sulfonate (PEDOT-PSS) can was made into stretchable electrodes only by the spin coating process [206]. The sheet resistance of the PEDOT: PSS is 46Ω/sq, which has been widely used in PLEDs [208], organic transistors [209] and flexible sensors [210]. However, the PEDOT: PSS electrode exhibits relatively low conductivity, which limits their further applications in IFS. In recent research, researchers usually used the doping process to improve the electrical conductivity of PEDOT: PSS electrodes [211]. For example, *LiPomi et al*. produced a stretchable electrode using PEDOT: PSS solution with azazolol and dimethyl sulfoxide [212]. Azazolol can increase the phase separation between the polyimetarhent acid ethylene glycol ester and the polystyrene chain to produce additional conducting paths. In addition, the mixture of PEDOT: PSS and metal-based nanomaterial can also effectively improve the conductivity and stretchability of the electrode. Compared to the original NWs electrodes, the surface roughness of the mixed electrode is significantly reduced, and the contact performance between NWs is

improved. As shown in Figure 9d, *Choi et al.* prepared a large area, smooth and flexible AgNW-PEDOT: PSS composite electrode [213]. The electrode had a transmittance of 84.3% and a sheet resistance of 10.76Ω/sq. After 200 cycles of stretching and folding, the sheet resistance of the composite electrode is only reduced by 5.3%. Recently, some researchers have also developed conductive polymers electrodes with electromagnetic shielding performance to shield electromagnetic interference and improve the stability of sensing performance [215]. For example, ultrathin flexible PVDF composite electrodes with MXenes and AgNWs were prepared based on solution casting method, which have good electrical conductivity, thermal conductivity, and electromagnetic shielding due to the synergistic effects induced by MXene/AgNWs network [216].

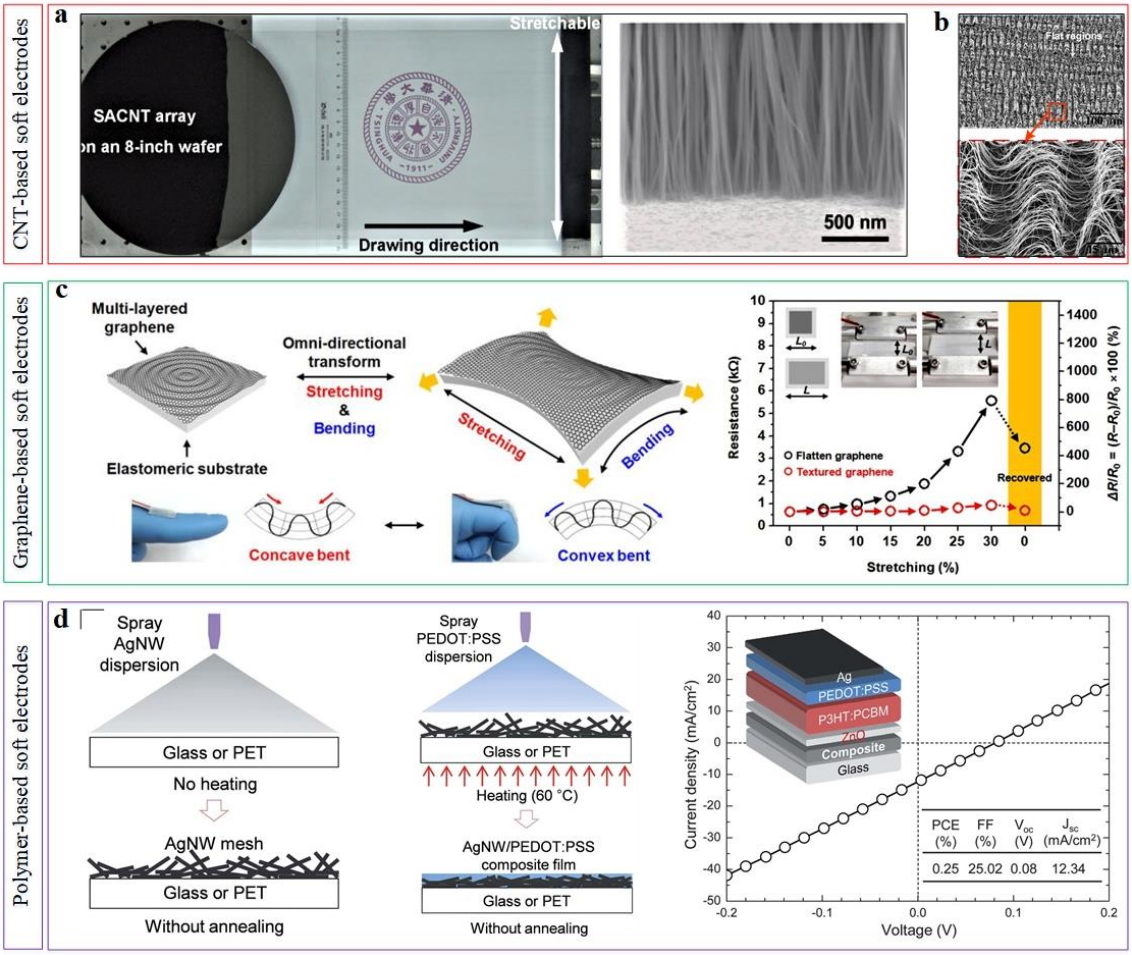

Figure 9. Non-metal-based electrodes. a) Carbon nanotube electrodes with vertical and parallel arrangement. Reproduced with permission.[198] Copyright 2010, Wiley-VCH. b) Carbon nanotube electrode with a wave shape. Reproduced with permission.[201] Copyright 2012, Wiley-VCH. c) Graphene electrode with a wave shape. Reproduced with permission.[164]

Copyright 2016, American Chemical Society. d) Electrode based on conducting polymer. Reproduced with permission.[213] Copyright 2012, Royal Society of Chemistry.

In recent years, some non-metal-based electrodes, such as ionic hydrogel and carbon nanotubes, also show some new characteristics, such as self-healing. [217]. Ionic hydrogel is often used as stretchable self-healing electrodes. Although the sheet resistance of ionic hydrogel is higher than that of metal conductors in general, it is still much lower than most of metal or non-metal conductors in stretched state. The nanopores inside the hydrogel are much larger than water molecule, and electrolytes or ionic liquids can flow inside it to achieve electrical signal transmission with high frequency [218, 219]. In addition, there are dynamic cross-linked chemical bonds inside the hydrogel, which can re-establish the molecular bond to achieve self-healing function. For example, *Te et al*. combined high-polar fluoroelastomers and fluorofluidic fluids to prepare a stretchable electrode with good self-healing function [220] (**Figure 10**a). Due to the interactions of ion and dipole, the electrode exhibited self-healing performance in dry and moist environments. Meanwhile, the electrode can operate at a strain of 30% and can repair the damaged area.

Besides the ionic hydrogel electrodes, the carbon nanotubes can also achieve self-healing function through a stacking process. Single-walled carbon nanotubes can be moved laterally in the surface of polymer matrix to repair the damaged area. Thus, single-walled carbon nanotubes are applied to the surface of polymer matrix with titanium dioxide nanospheres to form a self-healing electrode [221], as shown in Figure 10b. In addition, for the linear capacitive ionic sensor, the electrode is obtained by directional carbon nanotubes. When the microstructure of electrode is broken, the mutually aligned carbon nanotubes are reconnected by the lateral movement [222]. Recently, a self-healing electrode with liquid characteristics has been reported, as shown in Figure 10c [223]. An SH conductor comprising nickel flakes, eutectic gallium indium particles (EGaInPs), and carboxylated polyurethane are used as electrode materials. The hydrogen bond between the nitrogen hydride group and the carbon oxygen group promotes the self-healing and tensile properties, so that good conductivity can still be maintained under 700% tensile strain. Once being damaged, the liquid-metal particles are released from the oxide layer, and the nickel filler is attached to restore conductivity.

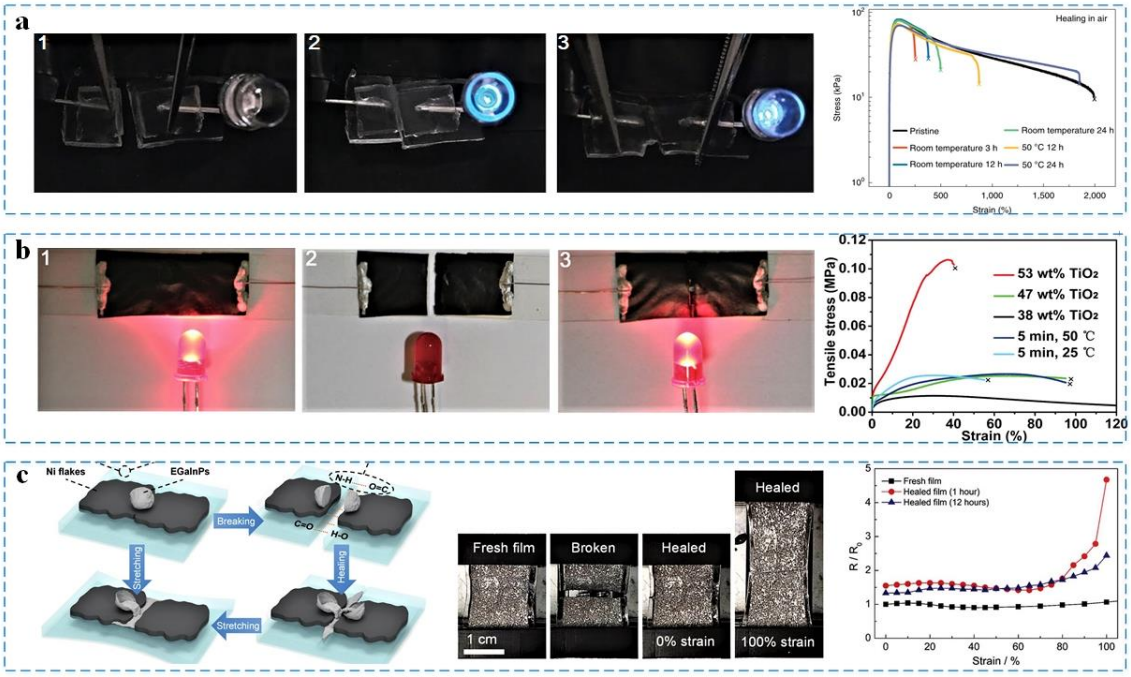

Figure 10. Self-healing electrodes. a) Ionic hydrogel electrodes with self-healing function. Reproduced with permission.[220] Copyright 2019, Macmillan. b) Carbon nanotube electrodes with self-healing function. Reproduced with permission.[221] Copyright 2014, Wiley-VCH. c) Self-healing electrodes with liquid characteristics. Reproduced with permission.[223] Copyright 2018, Wiley-VCH.

4. Structural optimization

According to the sensing model in the Section 2, the structure design and optimization of IFS is also crucial for the improvement of sensing performances, especially for the supercapacitive interfacial IFS. According to formula (1), the sensing performance depends on the contact area between electrode layer and ionic polymer matrix, which indicates that IFS need to have better compressibility for obtaining a broader contact area change. It is worth noting that although materials with a lower Young's modulus can provide outstanding flexibility and compressibility for IFS, the saturation of deformation takes place at a deformation in the material with a lower Young's modulus, which will result in smaller pressure range. Therefore, in practical, high sensitivity and broad pressure range are usually achieved through structural design and optimization of IFS, rather than reducing the Young's modulus of polymer matrix. Although there are many design methods for the structure

engineering of IFS, they can be roughly categorized into the surface structure and the internal structure, the purposes of which are to make IFS to achieve excellent flexibility and compressibility.

4.1 Polymer surface structure

Surface structure engineering refers to using the surface microstructure design of ionic polymer matrix to improve the sensitivity and response range of the sensor. These microstructures create the gaps between ionic polymer matrix and the electrodes to obtain good compressibility. First of all, the gaps reduce the rigidity of IFS. When the sensors are subjected to an external mechanical force, the contact area between the ionic polymer matrix and the electrodes is more likely to change. Secondly, because of the gaps, the initial contact area is very small, which makes the initial capacitive value of IFS very small. Therefore, IFS with the surface microstructures can further amplify the capacitance change, and improve the sensitivity and pressure range. In recent years, a variety of surface microstructures have been reported, such as pyramidal structure [224, 225], columnar structure [226, 227], fold structure [228, 229] and so on. These microstructures usually employed the similar preparation process. Firstly, a patterned silicon mold is made by photolithography, and then a wet or dry etching process is performed to form recessed microstructures. Then, the mixed liquid of gel and ionic electrolyte are casted on the silicon mold. Next, after vacuum degassing and annealing, an ionic gel film with surface microstructures is formed. As shown in **Figure 11**a1, *Cho et al*. used photolithography and KOH etching to prepare a mold with a pyramid array. Then a mixed solution of ionic liquid and PVDF-HFP polymer was poured into the mold. After vacuum degassing and annealing, a kind of ionic gel matrix with pyramidal microstructures on the surface was obtained. This ionic gel membrane showed excellent pressure sensing performance, including a broad pressure range (4 Pa~50 kPa), low working voltage (0.25V). Moreover, this sensor can achieve a sensitivity of 41kPa^{-1} below 400 Pa [230]. The reason is that each pyramidal tip has a square base with edges that are micrometers in length, tapering to a tip with a diameter of several hundreds of nanometers, which decreases elastic resistance, in turn improving sensitivity to pressure (Figure 11a2). Therefore, when the pyramidal microstructure is continuously compressed, the contact area between ionic polymer matrix

and the electrodes will continue to expand, which will result in the increase in capacitances. These IFS can effectively response to various pressures, including sound pressure, human pulse, and finger touch and so on. However, the preparation process of silicon molds is very complicated and expensive, so it cannot be effectively applied in practice.

Besides preparing the surface microstructures of ionic polymer matrix by using a silicon mold, many natural materials with microstructures on the surface can also be used to prepare the surface microstructures of ionic polymer matrix, such as petals [231], plant leaves [82], and fabric [19,232]. The lotus leaf is a natural material with super-hydrophobicity and self-cleaning performance, and its surface has a large number of micro-fuzz structures. *Wan et al*. used a cheap lotus leaf as a mold, and used polydimethylsiloxane (m-PDMS) to prepare a flexible matrix membrane. The surface of the membrane was covered with a large number of microstructures with high aspect ratios and low-density characteristics [233] (Figure 11b). Experiments showed that this sensor had ultra-high sensitivity ($1.2kPa^{-1}$) and ultra-low pressure response limit (0.8 Pa), which was an order of magnitude higher than the IFS with stable microstructures, such as columnar structure and pyramidal structure. The reason is that the compressibility of ionic polymer matrix is usually poor. As the sensor is compressed, the stable microstructure inevitably undergoes structural hardening. At this time, when higher pressure is applied, the sensor will undoubtedly decrease sensitivity. Instead, the surface microstructures with high aspect ratios will form height differences. When the sensor is subjected to external mechanical force, the electrode layer first contacts the highest layer of microstructures. Then as the pressure increases, the lower layer of microstructures will gradually contact the electrode layer, which will provide adequate space for further compression of the sensor. Therefore, IFS with the surface microstructures with high aspect ratios still have ultra-high sensitivity in a broad pressure range [234], as shown in Figure 11c. According to the same theory, *Bai et al.* used sandpaper as a mold to produce an ionic gel membrane with high aspect ratios and fillable structures. This structure presents fractal surface, which are easily compressed, deformed, and then fill in the groove when subjected to external mechanical force [235] (Figure 11d). The groove provides space for further compression of the sensor by accommodating the deformed microstructures. This IFS has a higher sensitivity (220-3300 kPa^{-1}) and high pressure resolution (about 10 Pa) in a broad

pressure range of up to 360 kPa.

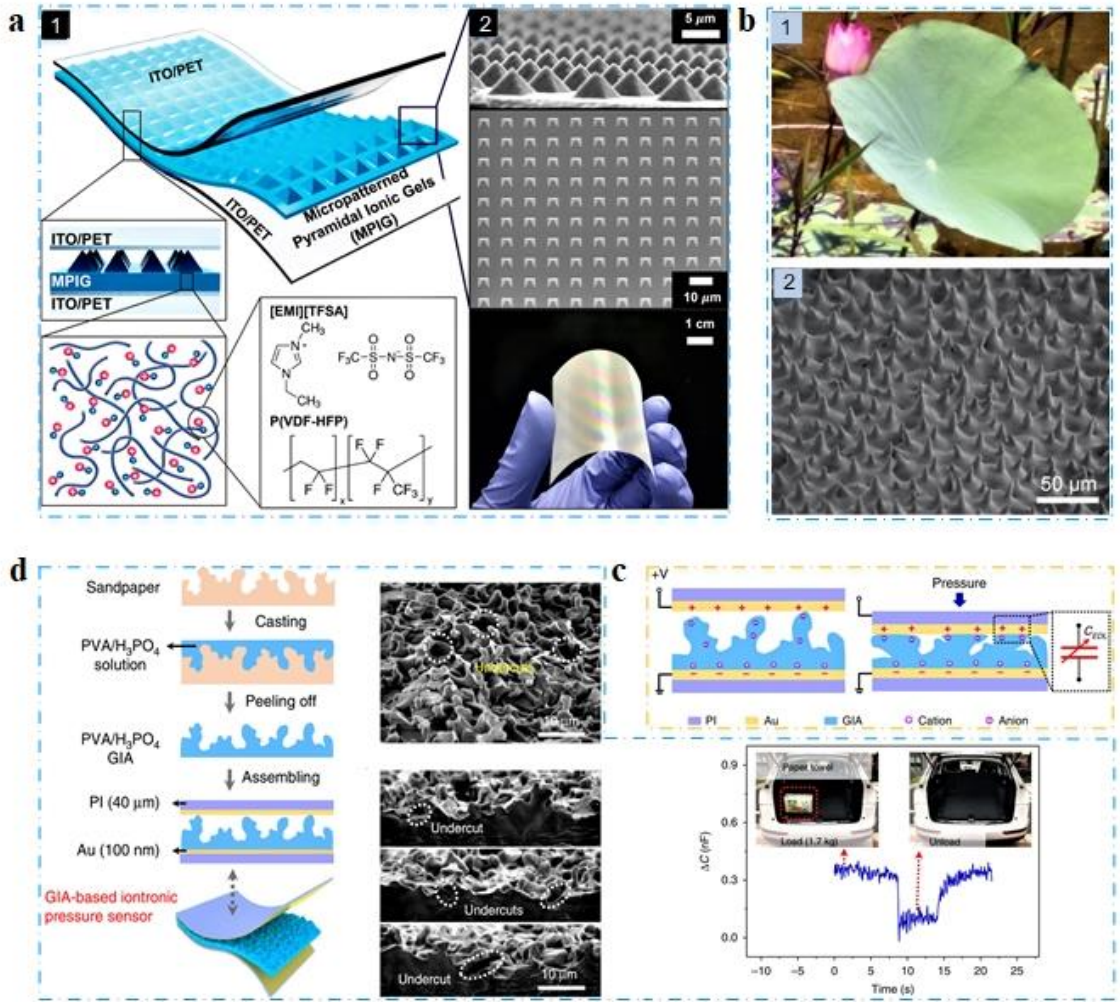

Figure 11. The surface structure engineering. a) IFS with pyramidal structure. Reproduced with permission.[230] Copyright 2017, American Chemical Society. b) IFS using a cheap lotus leaf as a mold. Reproduced with permission.[233] Copyright 2018, Wiley-VCH. c) Deformation mechanism of surface microstructures with high aspect ratios. d) IFS using a cheap sandpaper as a mold. Reproduced with permission.[235] Copyright 2020, Macmillan.

The surface microstructure design can not only effectively improve the sensitivity and pressure response range of IFS, but also make the sensor sense multiple types of strain [236, 237] and forces in different directions [238]. Recently, researchers used the ionic gel to prepare a kind of multi-modal tactile IFS with inverted pyramidal microstructures [239]. This sensor can respond to a variety of external mechanical forces, such as normal pressure, tangential force and torsion force. As shown in **Figure 12**a, when ionic polymer matrix is compressed by vertical pressure, the ionic gel is in contact with the bottom electrode. When the sensor is subjected to a shear force, ionic polymer matrix deforms and moves along the direction of

force, and finally contacts the side of the bottom electrode. When the sensor is subjected to a torsion force, ionic polymer matrix is in contact with the four sides of the bottom electrode. Compared with other classic sensors, the multi-modal tactile IFS does not need a complex integrated system or layered array structure, which indicates that the tactile IFS may replace various mechanoreceptors as an ideal sensing system for full-range tactile sensing.

Apart from the surface microstructure design of ionic polymer matrix, the surface microstructure design of the electrode has recently been reported [240]. As shown in Figure 12b, *Guo's* research team improved the compressibility of IFS by using soft micropillared electrodes with large height-to-radius aspect ratios, which was unstable and easy to bend. The micropillars undergo three stages of deformation upon loading, including initial contact (0-6 kPa), structure buckling (6-12 kPa) and post-buckling stage (12-176 kPa). Experiments showed that the sensor could have high linearity (R^2~0.999) and high sensitivity (33.16 kPa^{-1}) over a broad pressure range of 12~176 kPa [241]. The main reason is that the micropillars are prepared by the polydimethylsiloxane (PDMS) with an elastic modulus of 1 MPa, while the elastic modulus of the ionic gel membrane is 5 MPa. When the ionic gel membrane and the micropillars are squeezed by mechanical force of the MPa level, the ionic gel membrane will wrap the surface of the micropillars, which will make the contact area increase linearly.

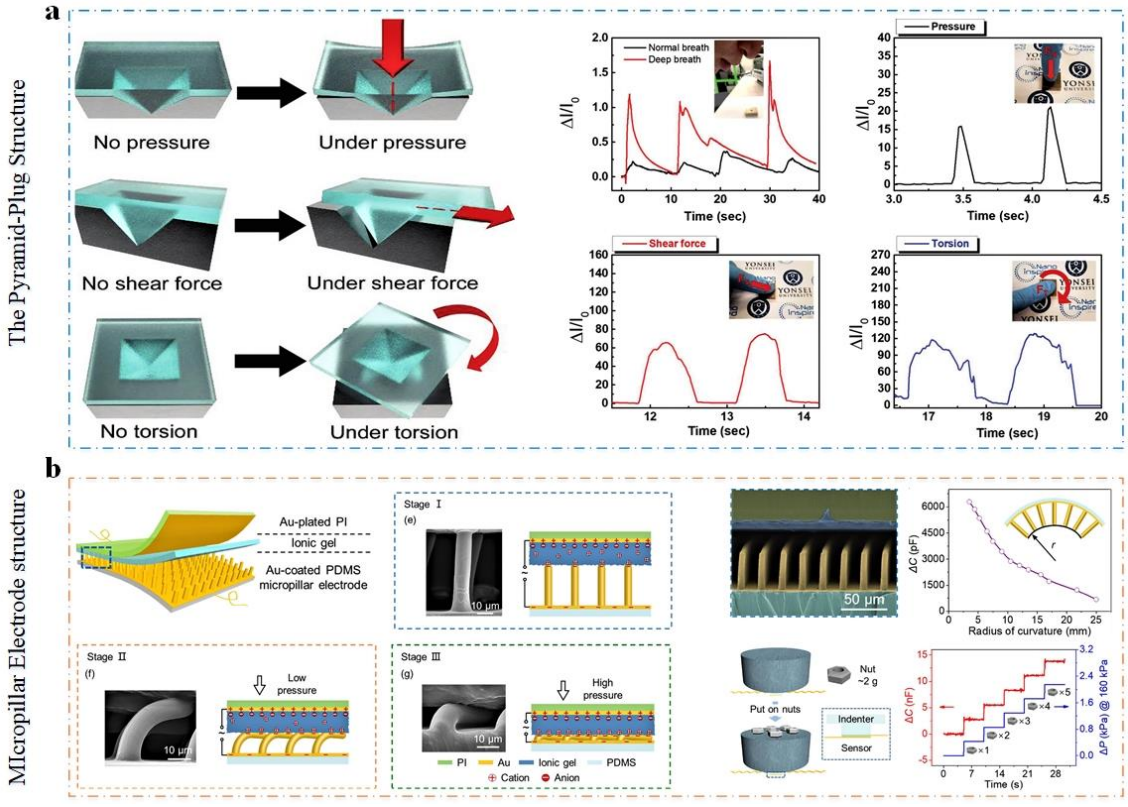

Figure 12. a) The multi-modal tactile IFS. Reproduced with permission.[239] Copyright 2018, Wiley-VCH. b) The electrode with the surface microstructure design. Reproduced with permission.[241] Copyright 2021, Elsevier.

4.2 polymer internal structure

Different from the surface structure, the internal structure mainly refers to preparing microporous structures inside the ionic polymer matrix to enhance the compressibility of ionic polymer matrix [242]. According to the compression theory of the microporous material, the deformation of IFS with microporous structures under the same external mechanical force can be shown in **Figure 13**a. Compared with the classical supercapacitive interfacial IFS, the Young's modulus of the IFS with microporous structures is usually low. Therefore, under the same external mechanical force, microporous structures can cause greater capacitance change. Furthermore, when the micropores are gradually shrunk, the effective dielectric constant will gradually increase. During the unloading process, the intrinsic stress of the elastic materials reopens the microporous structures and makes the capacitance of IFS to return to the initial state. In addition, the classical supercapacitive interfacial IFS will produce the bucket phenomenon under compression, which will cause interference to adjacent sensors in the array sensor. However, the microporous structures can provide enough space to suppress the bucket phenomenon. At present, many preparation methods of microporous structures have been reported. For example, ionic gel could be prepared into ionic fibers by an electrospinning process, which was then sandwiched between two electrodes to form supercapacitive interfacial IFS [35] (Figure 13b). Due to the large number of microporous structures inside the ionic fiber, it had good compressibility, excellent sensitivity and broad pressure range. In addition, this type of ionic fiber with microporous structures can also be obtained by mixing ionic gel and fabric [246]. *Zhou et al*. demonstrated of a pressure-sensitive nanofiber woven fabric sensor fabricated by weaving PVDF electrospun yarns of nanofibers coated with PEDOT. The nanofiber woven fabric sensor with multi-leveled hierarchical structure significantly induced the change in contact area under ultra-low load. Particularly, this wearable nanofiber woven fabric sensor showed combined superiority of high sensitivity (18.376 kPa^{-1}, at ~100 Pa), wide pressure range (0.002 – 10 kPa), fast response time (15 ms)

and better durability (7500 cycles) [227].

In addition to the ionic fiber, recently researchers have also studied the preparation process of directly generating microporous structures inside the ionic gel membrane, such as foam [243], sponge [244], paper fiber [36, 245], fabric [246] and so on. Pan et al. prepared IFS with internal microstructure through multiphase reaction [247]. The multiphase reaction made the inside of polypyrrole hydrogel form hollow sphere microstructure, which could cause IFS to have an ultra-low response limit (such as petals, about 0.8Pa). This had the advantages of short response time, good reproducibility, and high stability. In addition, *Kwon et al*. mixed the sugar cube and the ionic gel solution. After vacuum degassing and solidification, the sugar cube was dissolved in water to obtain an ionic gel membrane with microporous structures [248] (Figure 13c). The IFS had an ultra-high sensitivity of 0.6 kPa^{-1} at low pressure (< 5 kPa). It was suitable for general tactile pressure response, and the preparation technology was simple and low cost. In order to obtain higher sensitivity, the researchers combined the surface microstructure design with the internal microstructures to prepare a surface convex structure with micropores [249]. As shown in Figure 13d, *Yang et al*. used a photolithography process to prepare a pyramidal mold, then poured a mixed solution of polystyrene (PS) beads and PDMS into the mold and solidified to form pyramidal structures with micropores. Finally, toluene was used to dissolve the polystyrene (PS) beads [250]. Compared with the IFS with classical pyramidal structures, this kind of IFS had a sensitivity of 44.5kPa^{-1} under the pressure of less than 100Pa. This may be due to the advantages of the pyramidal microstructures and the microporous structures, which cause that the sensor has both a low elastic modulus and a larger change in dielectric constant.

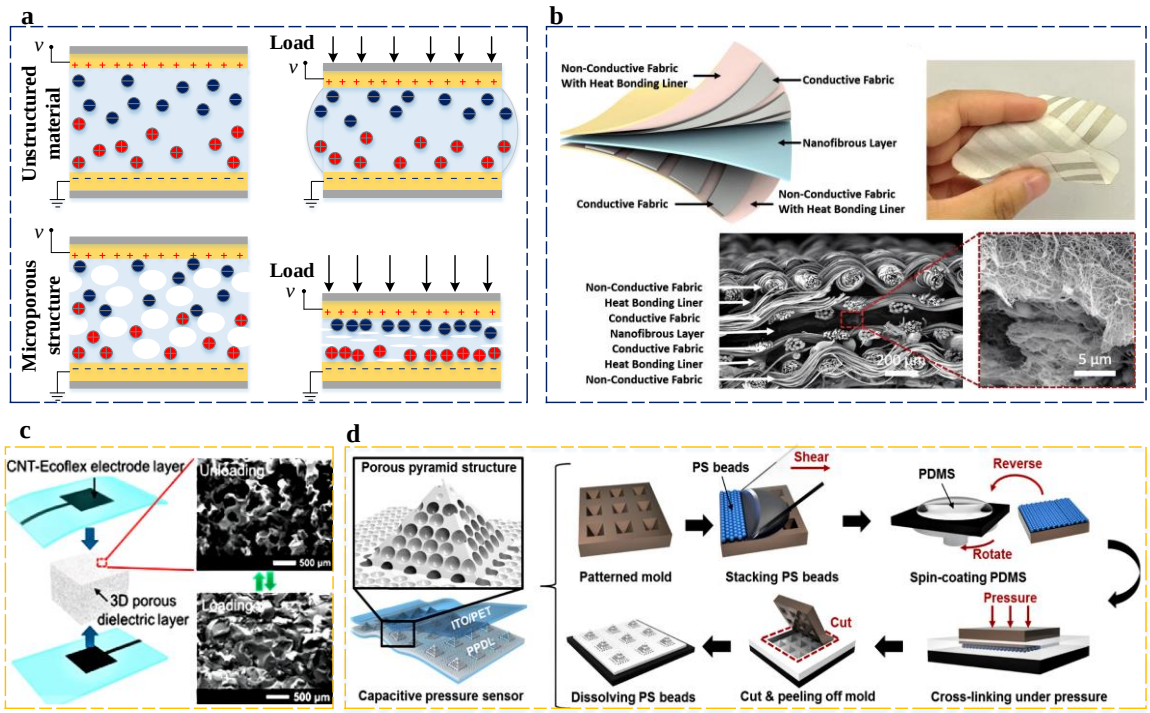

Figure 13. The internal structure engineering. a) Deformation mechanism of internal microstructure. b) IFS based on ionic fibers. Reproduced with permission.[35] Copyright 2017, Wiley-VCH. c) Hollow sphere microstructure is prepared by using sugar cube. Reproduced with permission.[248] Copyright 2016, American Chemical Society. d) A surface convex structure with micropores. Reproduced with permission.[250] Copyright 2019, American Chemical Society.

5. Applications

IFS represent a new category of flexible sensing devices, which not only have excellent mechanical flexibilities and high sensitivity, but also can mimic the biological mechanism of ion migration to achieve tactile perception functions like human skin. Compared with conventional flexible sensors, it can display more advanced biosensing interfaces, and lay a foundation for advanced technologies such as artificial skin, human-interactive technologies, and wearable health monitors.

5.1 Artificial skin

From the view of biological science, under external stimulation, ions in biological cells will flow out through ion channels, which can provide electrical signals to the nervous system

to sense external environment. Actually, artificial skin has excellent biocompatibility. However, it is a great challenge for conventional electronic skin [251]. Recently, many ionic materials have been used to realize artificial skin with the biocompatibility, such as ionic liquids, ionic gels, and ionic hydrogels. Similar to the sensing mechanism among biological cells, IFS uses movable ions to mimic the biological mechanism of ion migration [6], which can effectively sense pressure, strain, shear, torsion, and other external stimuli. Meanwhile, compared with conventional electronic skin composed of solid sensors, the former has the multimodality sensing capabilities and high stretchability. As shown in **Figure 14**, *Vipin Amoli et al.* used thermoplastic polyurethane (TPU) and silica aerosol to prepare an ionic sensor similar to a cell structure [252]. Figure 14a depicts the ion migration process of biological cells under external stimulation. It can be found that in the equilibrium state, the ion channel is closed and the concentration of positive and negative ions remains balanced inside and outside the cell membrane. When applying external mechanical force, ion channels on cell membrane are opened, and Na^+ in the extracellular matrix flows into the cells, which generates the electrical signals. Inspired by the structural and functional characteristics of biological cells, *Vipin Amoli et al.* used silica aerosol to mimic the cells in skin, and thermoplastic polyurethane (TPU) to mimic the cytoplasm in the skin (Figure 14b). In equilibrium state, anions and cations are adsorbed around silica aerosol by the non-covalent bonds. When IFS is subjected to external mechanical forces, the weak attraction between silica aerosol and ions is offset by mechanical stress and attracted by electric potential in the electrode layer to form EDL. After an external mechanical force is eliminated, free ions will return to an equilibrium state under the attraction of silica aerosol. In this artificial skin, breaking and rebuilding of H bonds between anions and silica and interaction of ions are similar to the previously reported self-healing polymers [253] and hydrogels [254]. This should be the reason for reversible movement of ions in supercapacitive interfacial IFS.

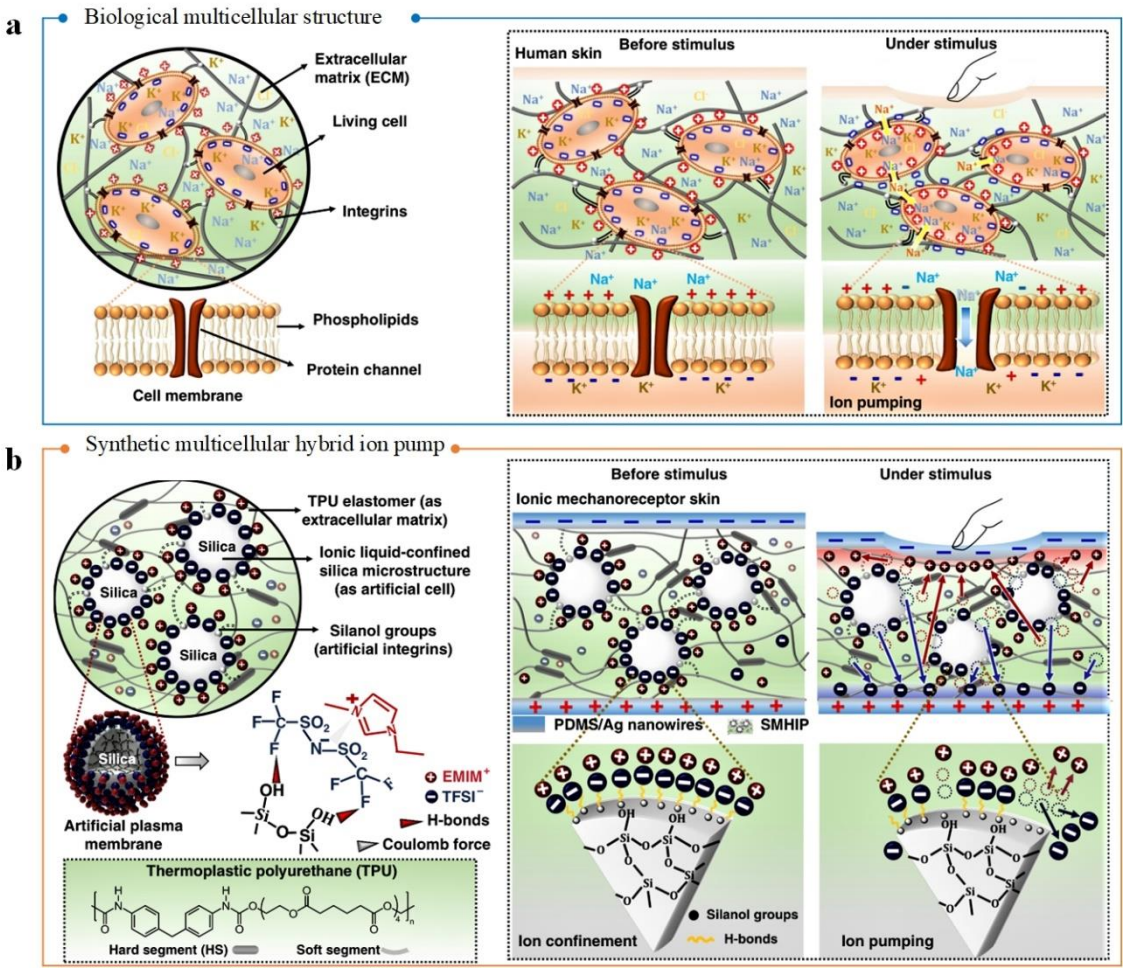

Figure 14. Artificial skin. a) Biological multicellular structure. b) Synthetic multicellular hybrid ionic pump. Reproduced with permission.[252] Copyright 2019, Macmillan.

In addition to the biocompatibility of artificial skin, how to use integration technology to form multi-touch sensing in large-area flexible sensors is also one of the main challenges of artificial skin [255]. Therefore, array integrated process has become another important research direction of artificial skin. Array structure design can be categorized into planar point structure and planar cross structure. The planar point structure usually refers to integration of several flexible sensors on a plane according to a certain rule. Each sensor has an independent surface electrode and circuit, and the sensors are relatively independent [256, 232]. For example, *Nie et al.* used ionic liquid as matrix material to make a new type of array supercapacitive interfacial IFS [9], in which each sensor element is relatively independent. Meanwhile, *Pang et al.* also used the same preparation method to make a 4x5 cm artificial skin with array sensors (**Figure 15**a). Experiments showed that tactile information, including position and pressure, can be determined by analyzing positive electrical signals recorded in real time [257]. However,

in this array structure, each sensor needs an independent signal transmission circuit and signal receiver, which will be a huge challenge for the design and implementation of the electrical system.

For planar cross structure, each sensing point is formed by superimposing two long strip sensors horizontally and vertically, and each sensor only needs a set of circuits and signal receivers. Horizontal and vertical sensors respectively determine the deformation positions in X and Y direction, and the position of force point can be determined according to coordinates in X and Y directions. This type of array structure is favored by many researchers [258, 259] due to its simple circuit and easy realization, as shown in Figure 15b. The long strip ionic sensors are placed crosswise to form array sensors with planar cross structures, which can accurately detect the position of pressure point [249]. In addition to directly using IFS to prepare the array sensors with planar cross structures, the cross-distributed electrodes were also prepared to form an artificial skin with array sensors. *Takei et al.* prepared an artificial skin with a 19×18 pixel array with the cross-distributed electrodes on surfaces of the flexible polymer matrix by a printing process (Figure 15c) [260]. In order to demonstrate the function of integrated artificial skin, research team formed a piece of polydimethylsiloxane (PDMS) with an area of about 3 cm^2 into a letter "C" and placed it on top of the array sensor. When applying a pressure (about 15kPa), this artificial skin can clearly sense the shape of objects. Pixels of this type of artificial skin are related to density of surface electrodes. In the future, pixel size can be easily reduced to the limit of lithography (for example, below 2μm) to achieve higher spatial resolution, which provides a feasible way for practical application of artificial skin.

Robotic prostheses can effectively restore human body's motion functions, which enable users to complete some tasks such as walking, grasping objects, and feeding. Although various types of prostheses have been developed, most prostheses are concentrated in the motion and lack of sensory function, which limits the tactile perception of amputees [5]. Installing an artificial skin with array sensors on surface of robot prosthesis can effectively help amputees perceive the external environment, including mechanical force, humidity [261], temperature [262, 263], and object shape. For example, researchers configured an ionic sensor with a three-dimensional microfluidic structure as a fingertip device, which could continuously sense the movement of fingertip, as well as magnitude and direction of external

mechanical strains [10]. In addition, with the advancement of ionic sensor technology, ionic artificial skin surpasses the human skin in terms of sensitivity and resolution. *Bai et al.* reported an intrafillable microstructure that can significantly improve sensitivity and response range of IFS [83]. Such intrafillable microstructures with undercuts and grooves that accommodate deformed surface microstructures effectively enhance the structural compressibility and the pressure response range. The intrafillable IFS exhibited an unprecedentedly high sensitivity (>220kPa $^{-1}$) over a broad pressure response range (0.08 Pa-360kPa), and an ultra-high pressure resolution (18Pa or 0.0056%) over the full pressure range.

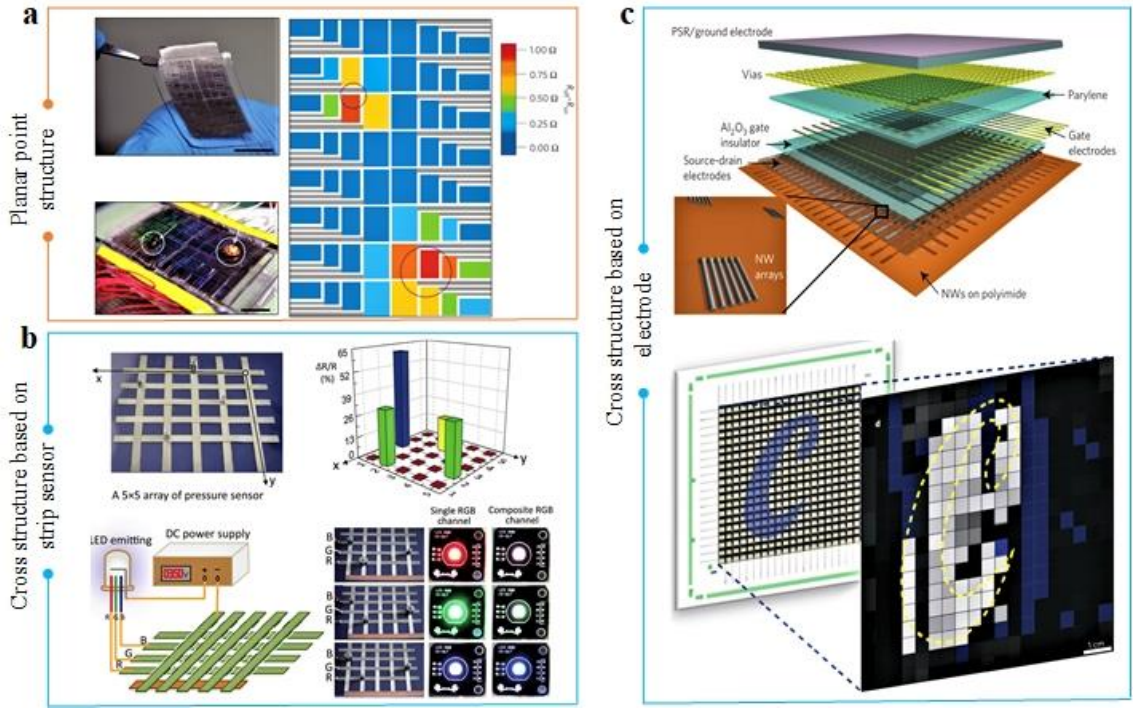

Figure 15. Array ionic sensors. a) Planar point structure. Reproduced with permission.[257] Copyright 2012, Macmillan. b) Cross structure based on strip sensors. Reproduced with permission.[249] Copyright 2016, Royal Society of Chemistry. c) Cross structure based on electrodes. Reproduced with permission.[260] Copyright 2010, Macmillan.

5.2 Human-interactive technologies

As introduced in section 5.1, the sensing function of IFS can be comparable to or even surpass that of biological skin, and capable of overcoming a technological challenge of the intimate communication between these flexible devices and biological systems [5]. IFS have

been used in the field of human-interactive technologies, including sports training, posture correction, gait analysis, rehabilitation training, and even for sign language [264, 265]. For instance, a flexible artificial skin with an inverted pyramid microstructure can be used as a fingertip sensor. Since inverted pyramid microstructure exhibits different deformation modes when subjected to different force, it can distinguish a variety of mechanical forces, such as normal force, shear force, torsion force [24]. Recently, a wearable ionic sensing glove for detecting human joints has also been reported [266]. As shown in **Figure 16**a, the sensing glove was composed of conducting fabric electrodes and silicone elastomer medium, which used a thermoplastic membrane to fuse conducting filaments to the conducting fabric electrode of the sensor. A soft and strong electrical connection was established to enable large strain range (~100% strain). The sensing glove can monitor finger movement and sense the posture of finger. Recently, with the development of advanced signal processing technologies, such as modern signal technology, artificial intelligence, and deep learning, IFS can also effectively monitor the movement angle and speed of human arms [267] (Figure 16b), gestures [268, 269] (Figure 16c), and braille recognition [9], etc.

Wearable IFS can convert human motion into electrical signals, which can also control robot through human motion. Various types of wearable IFS have been integrated with filter modules, microcontrollers, power supplies and wireless modules, and have been used to operate robotic arms or hands. As shown in Figure 16d, researchers prepared IFS with high sensitivity by a conducting fiber with excellent electrical properties and stability [270]. Then it was integrated into 6×6 pixel array sensors by weaving technology, and it was installed in gloves for wireless control of UAV and hexapod robots. In addition, IFS can also be directly used in soft grippers [271], soft robots [272], etc. The ionic sensor can perfectly adapt complex outer surface of the robot, adaptively deforming as robot operates, which is an advantage that conventional rigid sensors can hardly match.

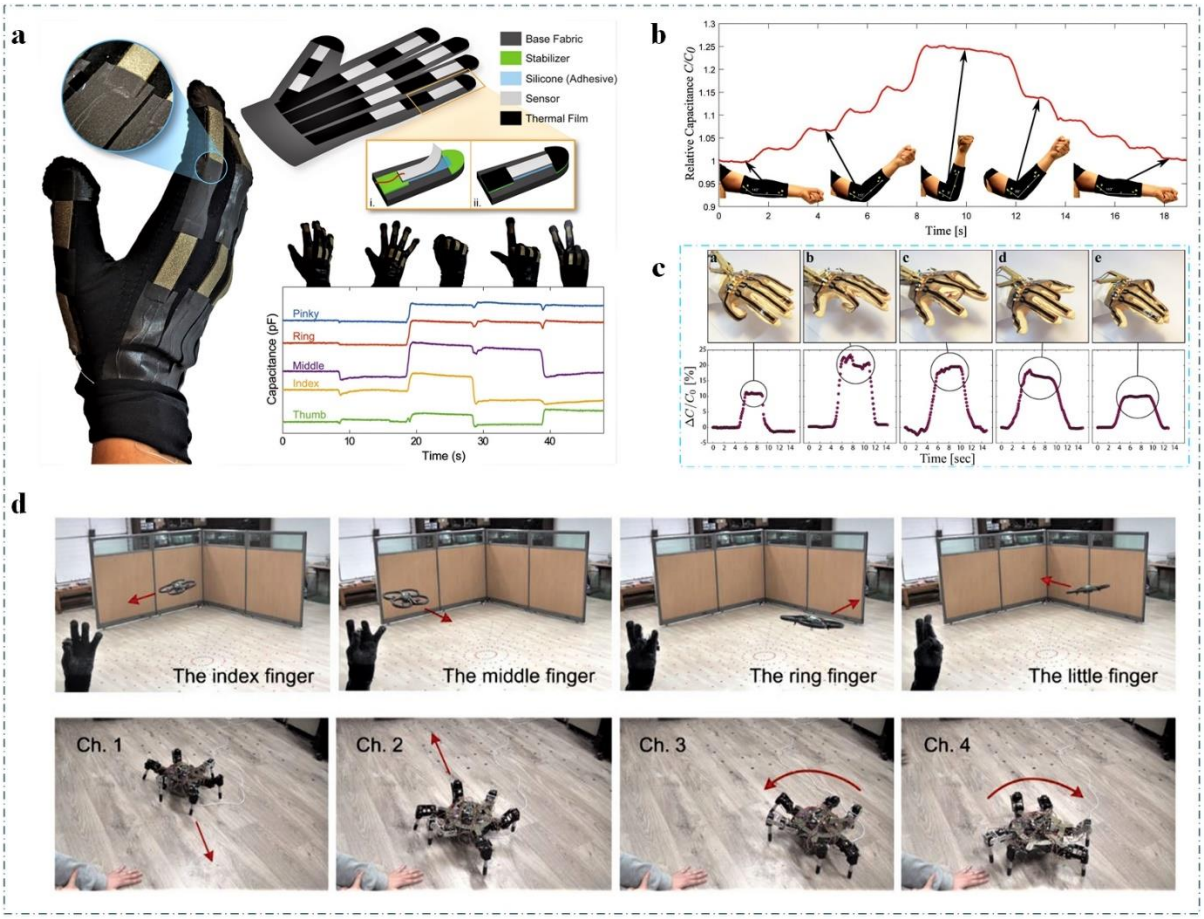

Figure 16. Human-interactive technologies equipment. a) The sensing glove. Reproduced with permission.[266] Copyright 2017, Wiley-VCH. b) IFS that can effectively monitor the movement angle and speed of human arms. Reproduced with permission.[267] Copyright 2017, Wiley-VCH. c) Gestures. Reproduced with permission.[269] Copyright 2018, Wiley-VCH. d) Wearable IFS that can control robot through human motion. Reproduced with permission.[270] Copyright 2015, Wiley-VCH.

5.3 Wearable health monitors

Currently, IFS have been applied to biomedical fields because of their good flexibility and biocompatibility to achieve remote and personalized health tests, including blood pressure monitoring, pulse monitoring, respiratory monitoring, and in vivo health monitoring [273, 274]. In particular, IFS can be used as non-invasive sensing devices that can adapt to human skin and obtain accurate biological and physiological signals.

In the medical field, arterial pulse can directly feedback various information about vascular health, including human exercise intensity [275, 276], physiological health, and so on.

For example, the frequency and amplitude of pulse will increase once the human are exercising. In addition, hardening of blood vessels will cause faster pulse and reflected waves will return early. Recently, different IFS have been used to monitor human pulse. However, the monitoring equipment must have a very small pressure response limit and high sensitivity due to low pulse amplitude of human pulse [277, 278]. As shown in **Figure 17**a, *Zhu et al*. prepared an ionic flexible pressure sensor with internal hollow structures [127]. This sensor could be placed on temples, neck, wrists, feet, chest, abdomen, and other places to monitor human pulse. Meanwhile, *B. Zhuo et al.* used ITO and PET as bottom and top electrode respectively to prepare an ionic sensor with surface microstructures by the 3D printing process for monitoring pulse rate [279]. The sensor had a sensitivity of 1.62 kPa^{-1} in pressure range of less than 0.2 kPa. The sensor together with data acquisition circuit has been well designed, but it cannot realize remote and personalized monitoring due to lack of wireless data transmission device.

Electrocardiogram can display the electrical signal of heart and provide information about heart beating process, which is very useful for predicting a serious heart attack. Especially patients and doctors can easily monitor the health of user's blood vessels by integrating sensors with wireless communication devices and display units. Figure 17b shows the monitoring system on human cardiovascular, including IFS, wireless communication devices and displays [280]. When heart rate is continuously monitored by the ECG ionic sensor, alarm platform of display screen is turned on or off according to the threshold of heart rate for the prevention and management of cardiovascular diseases. Lately, researchers have also applied ionic sensors to human respiratory monitoring to detect early respiratory diseases, including asthma, bronchitis, and sleep apnea [281]. As shown in Figure 17c, *S. Sharma et al.* integrated IFS into a mask to monitor human breathing [282]. Tested by subjects, it accurately showed that respiratory rate before and after exercise has increased from 24 to 48 times per minute. However, masks are not often needed, so it is necessary to design a more practical respiratory monitoring system, such as embedding sensors in textile clothing or affixed to the chest for respiratory monitoring [281, 283].

Plantar pressure can provides a quantity of information for footwear design, biomechanics, gait analysis, pre-diagnosis of foot-related diseases, and lower limb

rehabilitation (Figure 17d). However, feet bear the greatest pressure, which limits the use of most wearable sensors. Therefore, IFS with high sensitivity and a broad pressure response range need to have the ability to withstand maximum pressure for monitoring plantar pressure [284] (Figure 17e). Recently, researchers demonstrated a plantar pressure mapping system with an intelligent insole [285] (Figure 17f). The intelligent insole integrates Bluetooth technology and low-pass filtering technology to monitor plantar pressure in real time by transmitting signal to mobile phone. This work inspired application of IFS in footwear, which is of great significance for acquisition of human body information, injury prevention, and disease prediction. Besides, foot pulse signal of human is closely related to the health of whole body, which can further reflect the health information of human cardiovascular and skeletal muscle [286, 287]. *Pan's* research team integrated ionic sensors with shoe tongues to prepare five-unit array sensors for monitoring foot pulse signals and muscle activity [288]. Heart rate and breathing rate can be accurately recognized by capturing the foot pulse signal. Meanwhile, the movement posture of foot can also be accurately recognized by pressure change of foot.

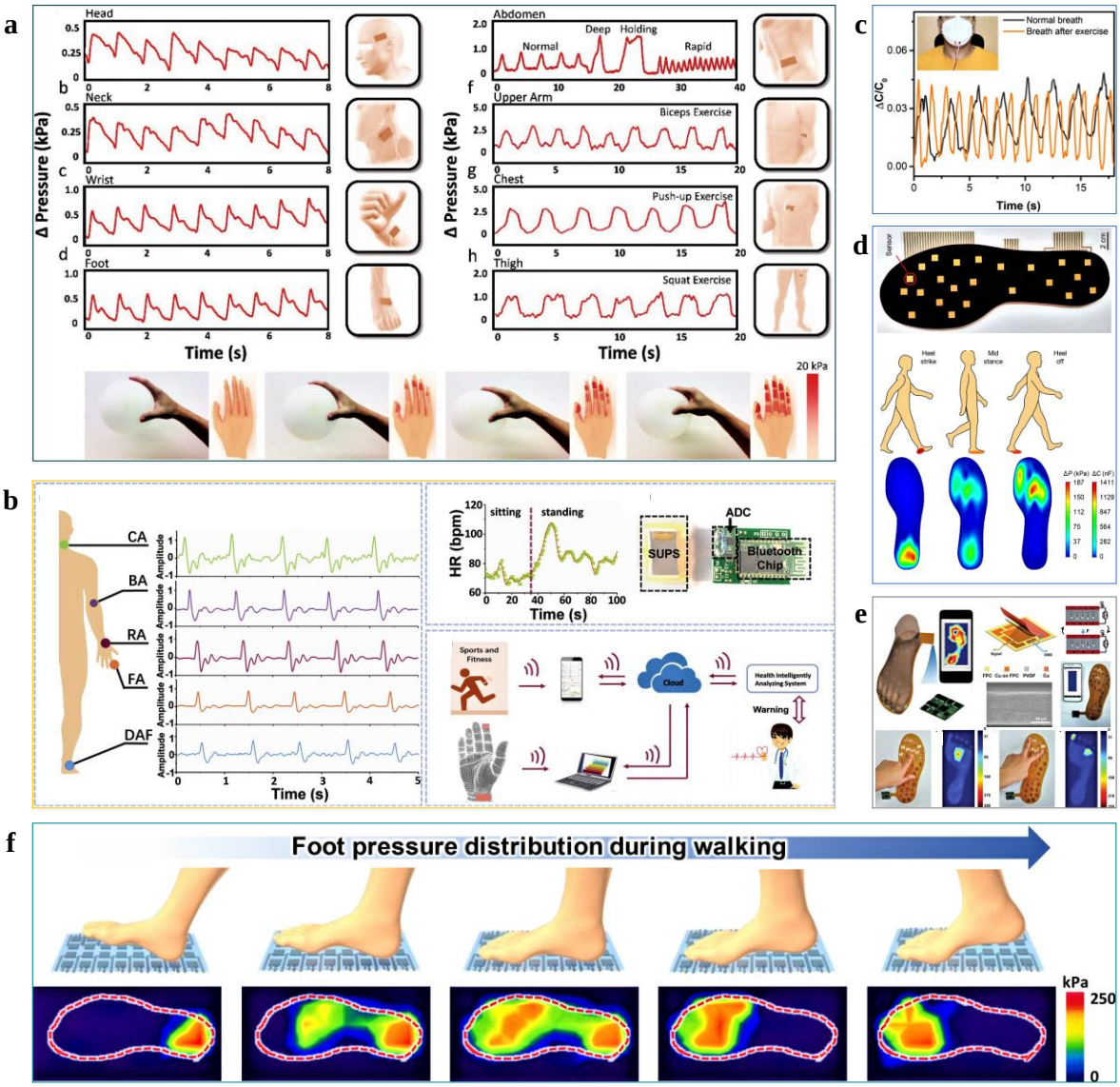

Figure 17. Wearable medical devices. a) IFS that can monitor human pulse. Reproduced with permission.[127] Copyright 2018, Wiley-VCH. b) The monitoring system about human cardiovascular. Reproduced with permission.[280] Copyright 2017, Wiley-VCH. c) Masks that can monitor human breathing. Reproduced with permission.[282] Copyright 2020, American Chemical Society. d）Plantar pressure sensor. Reproduced with permission.[241] Copyright 2021, Elsevier. e) Plantar pressure mapping system. Reproduced with permission.[285] Copyright 2018, Wiley-VCH. f) Intelligent insole. Reproduced with permission.[284] Copyright 2018, American Chemical Society.

Table 1. The summary and comparison of IFS with different mechanisms and materials

Mechanism	Compositions	Structure	Sensitivity	Response range	Mode of sensing	Characteristics	Ref.
Piezoresistive ionic sensing	PDES	Electrode with microstructure by 3D printing	348.28 kPa^{-1}	0.6 Pa-2000 kPa	Pressure	High sensitivity with ultrabroad-range	[240]
	DMAPS/MAA monomers			< 300 kPa	Pressure	Self-healing	[84]
	[OMIM][Cl]		0.1%	0.1–500%	Strain	Good durability	[289]
	[BMIM][Ntf2]/[BMIM][Ac]		40 (G.F.)	< 200%	Strain	Fast response	[290]
	EG/NaCl	Wavy-shaped hyperelastic channel	40 (G.F.)	< 800%	Strain		[61]
	Polyvinyl alcohol/fibers/ NaCl		2(G.F.)	< 300%	Strain	Good durability	[242]
	Ionic hydrogel		~0.78 (G.F.)	<300%	Strain	Stretchable and transparent	[275]
Supercapacitive interfacial ionic sensing	[EMIM][TFSI]/ PVDF-HFP	Multilayer surface microstructure by Sandpaper	11.73 kPa^{-1} (5-27.7 kPa)	1.12 Pa-32 kPa	Pressure		[62]
	Paper/[EMIM][TRIFLATE]/ PVA	Internal porous structure by paper	10 nF kPa^{-1}	< 100 kPa	Pressure	High linearity	[36]
	[EMIM][TFSI]/ TPU	Pyramidal microstructure by Silicon mold	43.6 kPa^{-1}	1 Pa-50 kPa	Pressure	High sensitivity	[74]
	[EMIM][TFSI]/ PVDF-HFP	Linear structure	9.62kPa^{-1} (0−40 kPa)	> 0.884 Pa	Pressure Strain	ultra-low response limit	[291]
	[EMIM][TFSI]/ PVDF-HFP	Multilayer double-sided microstructure by sandpaper	9.17 kPa^{-1}	0.013Pa~2063 kPa	Pressure	High linearity	[292]
	[BMIM]·PF6/Fabric	Internal porous structure by fabric	13.5 kPa^{-1}	< 13 kPa	Pressure	High resolution	[246]
	[BMIM]PF6/PVDF	Internal porous structure	1.194 kPa^{-1} (0–0.5 kPa) 0.109 kPa^{-1} (0.5–120 kPa)	0.4 Pa~ 120 kPa	Pressure	Good durability	[21]
	PVDF-co-HFP/ [EMIM][TFSI],	Pyramidal microstructure by silicon mold	10828 kPa^{-1}	1.1Pa~15kPa	Pressure	High sensitivity	[79]
	PVDF-HFP/ [EMIM][TFSI]	Microstructure with the high aspect ratio by sandpaper	145 kPa^{-1} (< 400Pa)	> 0.4 Pa	Pressure	Fast response	[234]
	RSF/ hydrogel /$CaCl_2$	Surface microstructure by fabric	0.20 kPa^{-1} (Pressure) 1.54%$^{\circ}C^{-1}$ (0–50°C)		Pressure, temperature	Good durability	[232]
	Melamine foam	Internal porous structure	1.285 kPa^{-1}	>0.5 Pa	Pressure	ultra-low response limit	[243]
	TPU/ [EMIM][TFSI]		2.65 nF kPa^{-1}	< 10 kPa	Pressure	All-Printed	[255]
	PVA/$H3PO_4$	Microstructure with a high aspect ratio by sandpaper	220 kPa^{-1}	0.08Pa-360 kPa	Pressure	High sensitivity with ultrabroad-range	[235]
	Ionic hydrogel		2 kPa^{-1}	<75 kPa	Pressure	High durability And stretchability	[77]
	PDMS/ MWCNTs	Internal porous structure by foam	0.01-0.02 kPa^{-1}	10 Pa-1.2 MPa	Pressure	ultrabroad-range	[244]
	Leaf/ PVDF-HFP/ [EMIM][TFSI]	Microstructure with a high aspect ratio by	54.31 kPa^{-1}	0.1 Pa-115 kPa	Pressure	High sensitivity	[82]
Piezoelectric ionic sensing	Nafion		0.798 pC/kPa		strain, pressure	High linearity	[45]
	Nafion		2.99mV		Strain	High stability	[51]

Nafion		200mV (1.6%)		Strain	High linearity	[293]
NaOH/ Nafion		< 0.4%		Strain	High sensitivity and linearity	[137]
PVDF/PANi/PCTE		<5.6 kPa $^{-1}$	< 20 kPa	Pressure		[294]
NaOH/ Nafion	Multilayer structure	< 0.53%		Strain	High linearity	[295]

6. Conclusions and Remarks

In this review, we summarize and discuss the progress of emerging ionic flexible sensors (IFS), including its sensing mechanisms, polymer matrix, electrodes, structural design, and potential applications. Generally, IFS can be categorized into supercapacitive interfacial IFS, piezoelectric IFS and piezoresistive IFS according to the sensing mechanisms and modes. The summary and comparison of IFS with different materials, structures, type of functions, and pressure/strain sensitivities are shown in Table 1. Firstly, as a dominant factor, the ionic material selection plays an influential role in determining the sensing performance and properties of IFS. Based on physical properties, they are further classified into ILs, ionic polymers/gels, hydrogels and nature-derived ionic materials, and described in this work in detail. In addition, the sensitivity and pressure response range of IFS could be dramatically enhanced through the structural design of ionic polymer matrix, and the stability and stretchability of IFS could be further improved through the optimization of ionic materials and electrodes, which have been included in the discussion according to different sensing modes, respectively. At the end of article, the prospects of IFS are discussed, and their challenges and opportunities in the artificial skin, human-interactive technologies, and wearable medical devices are intensively described. In particular, with recent interest and rapid progress in the development of IFS, it is exciting to see the new pressure-sensing modality possesses the major advantages of extremely high sensitivity, anti-interference, low detection noise and dynamic/static force response, which lay a foundation for the further development of electronic skin with good biological characteristics.

IFS have triggered the development of flexible sensors that extend beyond the natural tactile sensory capabilities of humans, but there are still many urgent challenges that need to be solved because they are in the initial stage of development. Firstly, although many sensing mechanisms and models of IFS have been reported in previous studies, they can only predict

the sensing performance of IFS in a specific environment, and not universal. It is difficult to accurately describe the mechanisms of IFS disturbed by external environment. In particular, the researches on certain factors are insufficient, such as water content, temperature, and humidity. Therefore, new sensing mechanisms and models of IFS should be further explored to adapt to IFS in various environments.

Furthermore, there have been many reports on ultra-sensitive IFS, but pressure response range of IFS needs to be further expanded, especially the ultra-low response limit, for meeting some specific demands in various applications, such as health monitoring, artificial skin, and prosthetics. Therefore, novel ionic materials and preparation processes should be further researched to achieve a tunable pressure response range. In addition, the sensing performance of IFS is affected by many factors, for example, the reduction of water content will cause sensing performance to degrade rapidly. Therefore, the stability of IFS is also a technical challenge. Although encapsulation process can effectively avoid the reduction of water content, conventional encapsulation process would decrease mechanical performance of IFS. Thence, advanced encapsulation technology should be further developed to reduce the impact of environment on IFS. At present, although IFS has experienced rapid development, the ionic sensing devices capable of sensing multiple forms have not been fully developed. Most of IFS have focused on the capability to sense only a single type of external mechanical stimulus. However, both biological skin and robot require a multimodal tactile sensing ability to sense multiple forces at the same time, such as tangential force, normal force, and torsion force. Therefore, structural design of IFS should be further developed or combined with advanced machine-learning techniques to distinguish the multiple mechanical forces.

In addition, In terms of preparation technology, several methods have been reported, including photolithography, mold, electroplating, printing, etc. Nonetheless, existing preparation process is complicated and expensive, and it is difficult to realize mass production of IFS. Meanwhile, the existing preparation process is not universal, which cannot prepare IFS with the same sensing performance even if using same preparation process. Moreover, with the rapid development of IFS over its first decade, IFS also has much additional functionality, such as biodegradable, self-powered and self-healing. However, for the optimal application of IFS with additional functionalities, numerous details such as the ionic materials, structure,

fabrication process, thickness, and encapsulation must be controlled to maintain the sensing performance, since adding functionalities may limit the material selection and fabrication process, which is also a technical challenge for the preparation process of IFS. Hence, it is necessary to develop a simple, low-cost, and universal preparation processes to make IFS fully develop from proof-of-concept devices in laboratory to commercial products.

7. References

[1]. R. Liu, G. Hu, M. Ban, Y. Zhang, L. Li, Y. Zhang, Nano Energy **2020**, 72, 104678.

[2]. A.S. Fiorillo, C.D. Critello, A.S. Pullano, Sensors and Actuators A: Physical **2018**, 281, 156-175.

[3]. X. Guo, G. Hu, Y. Zhang, R. Liu, M. Dan, L. Li, Y. Zhang, Nano Energy **2019**, 60, 36-42.

[4]. P. Zhu, Z. Zhao, J. Nie, G. Hu, L. Li, Y. Zhang, Nano Energy **2018**, 50, 744-749.

[5]. Y. Lee, J. Park, A. Choe, S. Cho, J. Kim, H. Ko, Adv. Funct. Mater. **2020**, 30, 1904523.

[6]. C. Yang, Z. Suo, Nat Rev Mater. **2018**, 3, 125–142.

[7]. B. Nie, S. Xing, J. D. Brandt, T. Pan, Lab Chip **2012**, 12, 1110.

[8]. X. Yang, S. Chen, Y. Shi, Z. Fu, B. Zhou, Sensors and Actuators A **2021**, 324, 112629.

[9]. B. Nie, R. Li, J. D. Brandt, T. Pan. Lab Chip **2014**, 14, 1107.

[10]. W. Zhang, N. Gao, J. Cui, C. Wang, S. Wang, G. Zhang, X. Dong, D. Zhang, G. Li, Chem. Sci. **2017**, 8, 6281-6289.

[11]. B. Nie, T. Yao, Y. Zhang, J. Liu, X. Chen, Appl. Phys. Lett. **2018**, 112, 031904.

[12]. H. Niu, S. Gao, W. Yue, Y. Li, W. Zhou, H. Liu, Small **2020**, 16, 1904774.

[13]. Z. Zhu, L. Chang, T. Horiuchi, K. Takagi, A. Aabloo, K. Asaka, Journal of Applied Physics **2016**, 119, 124901.

[14]. X. Liu, L. Yu, Z. Zhu, Y. Nie, A. L. Skov, Rapid Commun. **2021**, 42, 2000602.

[15]. Z. Zhu, T. Horiuchi, K. Kruusamae, L. Chang, K. Asaka, J. Phys. Chem. B **2016**, 120, 3215-3225.

[16]. S. Yamada, T. Sato, H. Toshiyoshi, Appl. Phys. Lett. **2017**, 110, 253501.

[17]. Y. Ren, Z. Liu, G. Jin, M. Yang, Y. Shao, W. Li, Y. Wu, L. Liu, F. Yan, Adv. Mater. **2021**, 33, 2008486.

[18]. J. Sun, G. Lu, J. Zhou, Y. Yuan, X. Zhu, J. Nie, ACS Appl. Mater. Interfaces **2020**, 12, 14272−14279.

[19]. Y. Wan, Y. Wang, C. F. Guo, Materials Today Physics. **2017**, 1, 61-73.

[20]. Q. Wang, M. Jian, C. Wang, Y. Zhang, Adv. Funct. Mater. **2017**, 27, 1605657.

[21]. Q. Liu, Z. Liu, C. Li, K. Xie, P. Zhu, B. Shao, J. Zhang, J. Yang, J. Zhang, Q. Wang, C. F. Guo, Adv. Sci. **2020**, 7, 2000348.

[22]. W. Hong, A. Almomani, R. Montazami, Measurement **2017**, 95, 128-134.

[23]. J. Wang, Y. Wang, Z. Zhu, J. Wang, Q. He, M. Luo, Sensors **2019**, 19(9), 2104.

[24]. Y. Wang, X. Cao, J. Cheng, B. Yao, Y. Zhao, S. Wu, B. Ju, S. Zhang, X. He, W. bin, ACS Nano **2021**, 15, 2, 3509–3521.

[25]. S. S. Patil, T. S. Bhat, A. M. Teli, S. A. Beknalkar, S. B. Dhavale, M. M. Faras, M. M. Karanjkar, P. S. Patil, Engineered Science **2020**, 12, 38-51.

[26]. R. Scaffaro, A. Maio, M. C. Citarrella, European Polymer Journal **2021**, 151, 110421.

[27]. L. Zhao, L. Wang, J. Shi, X. Hou, Q. Wang, Y. Zhang, Y. Wang, N. Bai, J. Yang, J. Zhang, B. Yu, C. F. Guo, ACS Nano **2021**, 15, 5752-5761.

[28]. L. Lin, Y. Xie, S. Wang, W. Wu, S. Niu, X. Wen, Z. L. Wang, ACS Nano **2013**, 7, 8266–8274.

[29]. V. Amoli, J. S. Kim, S. Y. Kim, J. Koo, Y. S. Chung, H. Choi, D. H. Kim, Adv. Funct. Mater. **2020**, 30, 1904532.

[30]. J. Kim, S. Lee, J. Hwang, E. Lee, K. Cho, S. Kim, D. H. Kim, W. H. Lee, Adv. Funct. Mater. **2020**, 30, 1908993.

[31]. Y. Chang, L. Wang, R. Li, Z. Zhang, Q. Wang, J. Yang, C. F. Guo, T. Pan, Adv. Mater. **2021**, 33, 2003464.

[32]. H.-J. Kim, K. Sim, A. Thukral, C. Yu, Sci. Adv. **2017**, 3, e1701114.

[33]. A. A. Kornyshev, J. Phys. Chem. B **2007**, 111, 5545-5557.

[34]. X. Yang, Y. Wang, X. Qing, Sensors **2018**, 18, 2395.

[35]. R. Li, Y. Si, Z. Zhu, Y. Guo, Y. Zhang, N. Pan, G. Sun, T. Pan, Adv. Mater. **2017**, 29, 1700253.

[36]. S. Li, N. Pan, Z. Zhu, R. Li, B. Li, J. Chu, G. Li, Y. Chang, T. Pan, Adv. Funct. Mater. **2019**, 29, 1807343.

[37]. H. Ota, K. Chen, Y. Lin, D. Kiriya, H. Shiraki, Z. Yu, T. Ha, A. Javey, Nat. Commun. **2014**, 5, 5032.

[38]. G. Meng, W. H. Ko, Sens. Actuators, A, **1999**, 75, 45.

[39]. S. Wang, L. Lin, Z. L. Wang, Nano Energy **2015**, 11, 436.

[40]. Y. Huang, X. Fan, S. C. Chen, N. Zhao, Adv. Funct. Mater. **2019**, 29, 1808509.

[41]. Y. Wang, H. Chen, Y. Wang, Z. Zhu, D. Li, Electrochimica Acta **2014**, 129, 450–458.

[42]. Y. Wang, J. Liu, Y. Zhu, D. Zhu, H. Chen, ACS Appl. Mater. Interfaces **2017**, 9, 30258–30262.

[43]. C. Jo, D. Pugal, Il-Kwon, K. J. Kim, K. Asaka, Progress in Polymer Science **2013**, 38, 1037-1066.

[44]. Z. Zhu, L. Chang, K. Asaka, J. Wang, H. Chen, H. Zhao, D. Li, Journal of Applied Physics **2014**, 115, 124903.

[45]. Y. Wang, Z. Zhu, J. Liu, L. Chang, H. Chen, Smart Mater. Struct. **2016**, 25, 085012.

[46]. Y. Wang, G. Tang, C. Zhao, K. Wang, J. Wang, J. Ru, J. Sheng, L. Chang, L. Li, Sensors and Actuators B: Chemical **2021**, 345, 130421.

[47]. X. He, X. Fang, B. Luo, H. Liu, C. Bian, Z. Zhu, IEEE Instrumentation & Measurement Magazine **2019**, 22, 13-23.

[48]. L. Chang, H. Chen, Z. Zhu, B. Li, Smart Mater. Struct. **2012**, 21, 065018.

[49]. M. A. Sharif, H. Lei, M. K. Al-Rubaiai, X. Tan, Smart Mater. Struct. **2018**, 27, 075039.

[50]. Z. Zhu, X. He, Q. He, X. Fang, Q. Hu, H. Chen, Journal of Applied Physics **2019**, 125, 024901.

[51]. Y. Ming, Y. Yang, R. P. Fu, C. Lu, L. Zhao, Y. M. Hu, C. Li, Y. X. Wu, H. Liu, W. Chen, Adv. Mater. Technol. **2018**, 3, 1800257.

[52]. G. Tang, Y. Wang, M. Hao , L. Zhang , J. Ru , L. Chang, L. Li, Smart Mater. Struct. **2021**, 30, 065013.

[53]. J.-H. Jung, J.-H. Jeon, V. Sridhar, Il-Kwon Oh. Chen, Carbon. **2011**, 49, 1279-1289.

[54]. Z. Zhu, C. Bian, J. Ru, W. Bai, H, Chen, Smart Mater. Struct. **2019**, 28, 01LT01.

[55]. Z. Zhu, T. Horiuchi, K. Kruusamae, L. Chang, K. Asaka, Smart Mater. Struct. **2016**, 25, 055024.

[56]. Z. Zhu, Y. Wang, Y. Liu, K. Asaka, X. Sun, L. Chang, P. Lu, Journal of Applied Physics **2016**, 120, 034901.

[57]. K. Kondo, K. Takagi, Z. Zhu, K. Asaka, Smart Mater. Struct. **2020**, 29, 115037.

[58]. J. Ru, Z. Zhu, Y. Wang, H. Chen, C. Bian, B. Luo, D. Li, Smart Mater. Struct. **2018**, 27 02LT01.

[59]. S. Li, H. Liu, Z. Zhu, X. Sun, Z. Tang, Y. Guo, Q. Hu, Y. Zhang, Smart Mater. Struct. **2021**, 30, 025004.

[60]. Z. Zhu, T. Horiuchi, K. Takagi, J. Takeda, L. Chang, K. Asaka, Journal of Applied Physics **2016**, 120, 084906.

[61]. D. Y. Choi, M. H. Kim, Y. S. Oh, S.-H. Jung, J. H. Jung, H. J. Sung, H. W. Lee, H. M. Lee, ACS Appl. Mater. Interfaces **2017**, 9, 1770.

[62]. A. Chhetry, J. Kim, H. Yoon, J. Y. Park, ACS Appl. Mater. Interfaces **2019**, 11, 3438.

[63]. J.-B. Chossat, Y.-L. Park, R. J. Wood, V. Duchaine, IEEE Sens. J. **2013**, 13, 3405.

[64]. Y. Zhu, C. Chao, C.-H. Cheng, W. W.-F. Leung, IEEE Electron Device Lett. **2009**, 30, 337.

[65]. N. Jiang, D. Hu, Y. Xu, J. Niu, D. Hu, Y. Xu, J. Chen, X. Chang, Y. Zhu, Y. Li, Z. Guo, Adv Compos Hybrid Mater. 2021, 4, 574–583.

[66]. C. Liu, S. Han, H. Xu, J. Wu, C. Liu, ACS Appl. Mater. Interfaces 2018, 10, 37, 31716–31724.

[67]. Y.-L. Park, B.-R. Chen, R. J. Wood, IEEE Sens. J. **2012**, 12, 2711.

[68]. J. H. Kim, K. G. Cho, D. H. Cho, K. Hong, K. H. Lee, Adv. Funct. Mater. **2021**, 31, 2010199.

[69]. G. Gao, F. Yang, F. Zhou, J. He, W. Lu, P. Xiao, H. Yan, C. Pan, T. Chen, Z. L. Wang, Adv. Mater. **2020**, 32, 2004290.

[70]. Y.-S. Ye, J. Rick, B.-J. Hwang, J. Mater. Chem. A **2013**, 1, 2719.

[71]. S. Z. Bisri, S. Shimizu, M. Nakano, Y. Iwasa, Adv. Mater. **2017**, 29, 1607054.

[72]. C. Angell, C. Liu, E. Sanchez, Nature **1993**, 362, 137.

[73]. K. Ueno, K. Hata, T. Katakabe, M. Kondoh, M. Watanabe, J. Phys. Chem. B **2008**, 112, 9013.

[74]. S. Jang, E. Jee, D. Choi, W. Kim, J. S. Kim, V. Amoli, T. Sung, D. Choi, D. H. Kim, J.-Y. Kwon, ACS Appl. Mater. Interfaces **2018**, 10, 31472.

[75]. R. Mohtadi, S.-i. Orimo, Nat. Rev. Mater. **2017**, 2, 16091.

[76]. Z. Li, S. Zhang, Y. Chen, H. Ling, L. Zhao, G. Luo, X. Wang, M. C. Hartel, H. Liu, Y. Xue, R. Haghniaz, K. Lee, W. Sun, H. Kim, J. Lee, Y. Zhao, Y. Zhao, S. Emaminejad, S. Ahadian, N. Ashammakhi, M. R. Dokmeci, Z. Jiang, A. Khademhosseini, Adv. Funct. Mater. **2020**, 2003601.

[77]. W. Xie, J. Duan, H. Wang, J. Li, R. Liu, B. Yu, S. Liua, J. Zhou, J. Mater. Chem. A, **2018**, 6, 24114-24119.

[78]. E. M. Ahmed. J. Adv. Res. **2015**, 6, 105.

[79]. S. Chen, A. Surendran, X. Wu, W. L. Leong, Adv. Funct. Mater. **2020**, 30, 2006186.

[80]. B. Nie, R. Li, J. Cao, J. D. Brandt, T. Pan, Adv. Mater. **2015**, 27, 6055.

[81]. S. Zhang, F. Wang, H. Peng, J. Yan, G. Pan, ACS Omega **2018**, 3, 3014.

[82]. Z. Qiu, Y. Wan, W. Zhou, J. Yang, J. Yang, J. Huang, J. Zhang, Q. Liu, S. Huang, N. Bai, Z. Wu, W. Hong, H. Wang, C. F. Guo, Adv. Funct. Mater. **2018**, 28, 1802343.

[83]. W. Y. Lee, Y. M. Kim, J. H. Kwon, H. C.l Moon. J. Mater. Chem. C, **2021**, 9, 5445-5451

[84]. Z. Lei, P. Wu, ACS Nano **2018**, 12, 12860−12868.

[85]. A. Manthiram, X. Yu, S. Wang, Nat. Rev. Mater.**2017**, 2, 16103.

[86]. M. S. Sarwar, Y. Dobashi, C. Preston, J. K. M. Wyss, S. Mirabbasi, J. D. W. Madden, Science Advances, **2017**, 3, e1602200.

[87]. Z. Lei, P. Wu, Nat. Commun. **2018**, 9, 1134.

[88]. C. H. Yang, S. Zhou, S. Shian, D. R. Clarke, Z. Suo, Mater. Horiz. **2017**, 4, 1102–1109.

[89]. C.-C. Kim, H.-H. Lee, K. H. Oh, J.-Y. Sun, Science **2016**, 353, 682–687.

[90]. J. Yang, T. Hong, J. Deng, Y. Wang, F. Lei, J. Zhang, B. Yu, Z. Wu, X. Zhang, C. F. Guo, Chem. Commun. **2019**, 55, 13737-13740.

[91]. S. G. Yoon, B. J. Park, S. T. Chang, ACS Appl. Mater. Interfaces **2017**, 9, 36206.

[92]. J.-Y. Sun, C. Keplinger, G.M. Whitesides, Z. Suo, Adv. Mater. **2014**, 26: 7608-7614.

[93]. W. G. Moon, G.-P. Kim, M. Lee, H. D. Song, J. Yi, ACS Appl. Mater. Interfaces **2015**, 7, 3503.

[94]. Y. N. Sudhakar, M. Selvakumar, D. K. Bhat, Ionics **2013**, 19, 277.

[95]. H. Yang, Y. Liu, L. Kong, L. Kang, F. Ran, J. Power Sources **2019**, 426, 47.

[96]. Y. Li, J. Guo, M. Li, Y. Tang, V. Murugadoss, I. Seok, J. Yu, L. Sun, C. Sun, Y. Luo, ES Food &

Agroforestry **2021**, 4, 9-27.

[97]. L. Xiao, H. Qi, K. Qu, C. Shi, Y. Cheng, Z. Sun, B. Yuan, Z. Huang, D. Pan, Z. Guo, Adv Compos Hybrid Mater **2021**, 4, 306–316.

[98]. K. Qu, Z. Sun, C. Shi, W. Wang, L. Xiao, J. Tian, Z. Huang, Z. Guo, Adv Compos Hybrid Mater. **2021**, 4, 670–683.

[99]. Y. H. Jung, T.-H. Chang, H. Zhang, C. Yao, Q. Zheng, V. W. Yang, H. Mi, M. Kim, S. J. Cho, D.-W. Park, H. Jiang, J. Lee, Y. Qiu, W. Zhou, Z. Cai, S. Gong, Z. Ma, Nat. Commun. **2015**, 6, 7170.

[100]. X. Gao, L. Huang, B. Wang, D. Xu, J. Zhong, Z. Hu, L. Zhang, J. Zhou, ACS Appl. Mater. Interfaces **2016**, 8, 35587.

[101]. Q. Zhang, C. Chen, W. Chen, G. Pastel, X. Guo, S. Liu, Q. Wang, Y. Liu, J. Li, H. Yu, L. Hu, ACS Applied Materials & Interfaces **2019**, 11, 5919-5927.

[102]. D. Zhao, C. Chen, Q. Zhang, W. Chen, S. Liu, Q. Wang, Y. Liu, J. Li, H. Yu, Adv. Energy Mater. **2017**, 7, 1700739.

[103]. J. Deng, H. Yuk, J. Wu, C. E. Varela, X. Chen, E. T. Roche, C. F. Guo, X. Zhao, Nat. Mater. **2021**, 20, 229–236.

[104]. M. I.-Vladu, Chem. Soc. Rev. **2014**, 43, 588.

[105]. H. Liu, D. Xu, B. Hu, J. Jiang, M. Li, D. Zhao, W. Zha, J. Mater. Chem. A, **2021**, 9, 4692–4699.

[106]. X. Wang, W. Xu, P. Chatterjee, C. Lv, J. Popovich, Z. Song, L. Dai, M. Y. S. Kalani, S. E. Haydel, H. Jiang, Adv. Mater. Technol. **2016**, 1, 1600059.

[107]. M. Hu, J. Wang, J. Liu, P. Wang, Y. Feng, H. Wang, N. Nie, Y. Wang, Y. Huang, Energy Storage Mater. **2019**, 21, 174.

[108]. K. K. Fu, Z. Wang, J. Dai, M. Carter, L. Hu, Chem. Mater. **2016**, 28, 3527.

[109]. X. Yu, W. Shou, B. K. Mahajan, X. Huang, H. Pan, Adv. Mater. **2018**, 30, 1707624.

[110]. G. Lee, S.-K. Kang, S. M. Won, P. Gutruf, Y. R. Jeong, J. Koo, S. - S. Lee, J. A. Rogers, J. S. Ha, Adv. Energy Mater. **2017**, 7, 1700157.

[111]. M. Burnworth, L. Tang, J. R. Kumpfer, A.J. Duncan, F. L. Beyer, G. L. Fiore, S. J. Rowan, C. Weder, Nature **2011**, 472, 334–337.

[112]. B. Ghosh, M. W. Urban, Science **2009**, 323, 1458–1460.

[113]. K. S. Toohey, N. R. Sottos, J. A. Lewis, J. S. Moore, S. R. White, Nature Mater **2007**, 6, 581–585.

[114]. M. M. Caruso, D. A. Delafuente, V. Ho, N. R. Sottos, J. S. Moore, S. R. White, Macromolecules

2007, 40, 8830-8832.

[115]. A.C. Jackson, J.A. Bartelt, P.V. Braun, Adv. Funct. Mater. **2011**, 21, 4705-4711.

[116]. S. R. White, N. R. Sottos, P. H. Geubelle, J. S. Moore, M. R. Kessler, S. R. Sriram, E. N. Brown, S. Viswanathan, Nature **2001**, 409, 794.

[117]. L. Wang, G. Gao, Y. Zhou, T. Xu, J. Chen, R. Wang, R. Zhang, J. Fu, ACS Appl. Mater. Interfaces **2019**, 11, 3, 3506–3515.

[118]. Y. Ding, H. Tang, C. Zhang, W. Li, G. Li, Y. Zhang, C. Xu, F. Zhao, Q. Guo, C. F. Guo, X.-D. Xiang, Adv. Funct. Mater. **2021**, 31, 2100489.

[119]. Z. Zhang, L. Wang, H. Yu, F. Zhang, L. Tang, Y. Feng, W. Feng, ACS Appl. Mater. Interfaces **2020**, 12, 15657–15666.

[120]. S. Tang, B. M. Richardson, K. S. Anseth, Progress in Materials Science **2021**, 120, 100738.

[121]. Y. Lin, H. Zhang, H. Liao, Y. Zhao, K. Li, Chem. Eng. J. **2019**, 367,139.

[122]. M. Krogsgaard, M. A. Behrens, J. S. Pedersen, H. Birkedal, Biomacromolecules **2013**, 14, 297−301.

[123]. J. Yin, S. Pan, L. Wu, L. Tan, D. Chen, S. Huang, Y. Zhang, P. He, J. Mater. Chem. C, **2020**, 8, 17349-17364.

[124]. X. Yang, J. Liu, D. Fan, J. Cao, X. Huang, Z. Zheng, X. Zhang, Chemical Engineering Journal **2020**, 389, 124448.

[125]. S. Basak, J. Nanda, A. Banerjee, Chem. Commun. **2014**, 50, 2356-2359.

[126]. C.-H. Li, C. Wang, C. Keplinger, J.-L. Zuo, L. Jin, Y. Sun, P. Zheng, Y. Cao, F. Lissel, C. Linder, X.-Z. You, Z. Bao, Nature Chem **2016**, 8, 618–624.

[127]. Z. Zhu, R. Li, T. Pan, Adv. Mater. **2018**, 30, 1705122.

[128]. Y. Zhang, S. Sezen, M. Ahmadi, X. Cheng, R. Rajamani, Sci. Rep. **2018**, 8, 16284.

[129]. J. Yang, Q. Liu, Z. Deng, M. Gong, F. Lei, J. Zhang, X. Zhang, Q. Wang, Y. Liu, Z. Wu, C.F. Guo, Materials Today Physics. **2019**, 8, 78-85.

[130]. Y. Wan, Z. Qiu, J. Huang, J. Yang, Q. Wang, P. Lu, J. Yang, J. Zhang, S. Huang, Z. Wu, C. F. Guo, Small **2018**, 14, 1801657.

[131]. L.-Q. Tao, K.-N. Zhang, H. Tian, Y. Liu, D.-Y. Wang, Y.-Q. Chen, Y. Yang, T.-L. Ren, ACS Nano **2017**, 11, 8790-8795.

[132]. S. Gong, W. Schwalb, Y. Wang, Y. Chen, Y. Tang, J. Si, B. Shirinzadeh, W. Cheng, Nat Commun **2014**, 5, 3132.

[133]. K.-I. Jang, S. Y. Han, S. Xu, K. E. Mathewson, Y. Zhang, J.-W. Jeong, G.-T. Kim, R C. Webb, J.W. Lee, T. J. Dawidczyk, R. H. Kim, Y. M. Song, W.-H. Yeo, S. Kim, H. Cheng, S. Il Rhee, J. Chung, B. Kim, H. U. Chung, D. Lee, Y. Yang, M. Cho, J. G. Gaspar, R. Carbonari, M. Fabiani, G. Gratton, Y. Huang, J. A. Rogers, Nat Commun **2014**, 5, 4779.

[134]. S. Choi, Z. Jiang, Sensors and Actuators A **2006**, 128, 317-326.

[135]. J. Coosemans, B. Hermans, R. Puers, Sensors and Actuators A **2006**, 130, 48-53.

[136]. J. Löfhede, F. Seoane, M. Thordstein, Sensors **2012**, 12, 16907-16919.

[137]. S. Han, J. Zhao, D. Wang, C. Lu, W. Chen, J. Mater. Chem. B, **2017**, 5, 7126-7132.

[138]. J. Ru, Z. Zhu, Y. Wang, H. Chen, D. Li, RSC Adv., **2018**, 8, 3090-3094.

[139]. J. Ru, Y. Wang, L. Chang, H. Chen, D. Li, Smart Mater. Struct. **2016**, 25, 095006.

[140]. Y. Wang, Z. Zhu, H. Chen, B. Luo, L. Chang, Y. Wang, D. Li, Smart Mater. Struct. **2014**, 23, 125015.

[141]. K. J. kim, M. Shahinpoor, Polymer **2002**, 43, 797-802.

[142]. S. J. Lee, M. J. Han, S. J. Kim, J. Y. Jho, H. Y. Lee, Y. H. Kim, Smart Mater. Struct. **2016**, 15 1217.

[143]. Z. Zhu, L. Chang, K. Takagi, Y. Wang, H. Chen, D. Li, Appl. Phys. Lett. **2014**,105, 054103.

[144]. D. Zhao, D. Li, Y. Wang, H. Chen, Smart Mater. Struct. **2016**, 25, 075043.

[145]. V. K. Nguyen, J. W. Lee, Y. Yoo, Sensors and Actuators B **2007**, 120, 529–537.

[146]. D. Y. Lee, Il-S. Park, M.-H. Lee, K. J. Kim, S. Heo, Sensors and Actuators A **2007**, 133, 117–127

[147]. S. Liu, Y. Liu, H. Cebeci, R.G. Villoria, J. ‐ H. Lin, B.L. Wardle, Q.M. Zhang, Adv. Funct. Mater. **2010**, 20, 3266-3271.

[148]. A. Khan, R. K. Jain, B. Ghosh, Inamuddin, A. M. Asiri, RSC Adv. **2018**, 8, 25423-25435.

[149]. I. Oh, J. Jung, J. Jeon, S. Vadahanambi, Smart Mater. Struct. **2010**, 19, 075009.

[150]. B. Luo, H. Chen, Z. Zhu, B. Xie, C. Bian, Y. Wang, Materials & Design. **2018**, 155, 125-133.

[151]. Y. Tang, C. Chen, Y. S. Ye, Z. Xue, X. Zhou, X. Xie, Polym. Chem. **2014**, 5, 6097.

[152]. Y. Tang, Z. Xue, X. Zhou, X. Xie, C.-Y. Tang, Sensors and Actuators B **2014**, 202, 1164-1174.

[153]. J.-H. Jeon, S.-P. Kang, S. Lee, Il-K. Oh, Sensors and Actuators B **2009**, 143, 357–364.

[154]. H. M. Jeong, S. M. Woo, S. Lee, G. Cha, M. S. Mun, J. Appl. Polym. Sci. **2005**, 99, 1732-1739.

[155]. J. Y. Lee, H. S. Wang, B. R. Yoon, M. J. Han, J. Y. Jho, Rapid Commun. **2010**, 31, 1897-1902.

[156]. X.-L. Wang, Il-K. Oh, S. Lee, Sensors and Actuators B **2010**, 150: 57-64.

[157]. S. Huang, Y. Liu, Y. Zhao, Z. Ren, C. F. Guo, Adv. Funct. Mater. **2019**, 29, 1805924.

[158]. T. Li, Y. Li, T. Zhang, Accounts of Chemical Research **2019**, 52, 288-296.

[159]. P. Peng, K. Wu, L. X. Lv, C. F. Guo, Z. G. Wu, Adv. Mater. Technol. **2018**, 3, 1700264.

[160]. S. Zhang, J. Jiang, Q. Jiang, W. Fei, C. F. Guo, Z. Wu, Adv. Mater. Technol. **2021**, 6, 2001274.

[161]. Y. Ma, X. Xie, W. Yang, Z. Yu, X. Sun, Y. Zhang, X. Yang, H. Kimura, C. Hou, Z. Guo, W. Du, Adv Compos Hybrid Mater., Doi:10.1007/s42114-021-00358-2.

[162]. N. S. Korivi, M. Vangari, L. Jiang, Applied Nanoscience **2017**, 7, 41–45.

[163]. C. Bian, J. Ru, Z. Zhu, B. Luo, H. Chen, Smart Mater. Struct. **2018**, 27, 085017.

[164]. J.-Y. Hong, W. Kim, D. Choi, J. Kong, H. S. Park, ACS Nano, **2016**, 10, 9446.

[165]. J. Mu, C. Hou, G. Wang, X. Wang, Q. Zhang, Y. Li, H. Wang, M. Zhu, Adv. Mater.**2016**, 28, 9491.

[166]. Y. Wang, N. Bai, J. Yang, Z. Liu, G. Li, M. Cai, L. Zhao, Y. Zhang, J. Zhang, C. Li, Y. Zhou, C. F. Guo, Journal of Materiomics. **2020**, 6, 152-157.

[167]. Y. Wang, T. Hong, L. Wang, G. Li, N. Bai, C. Li, P. Lu, M. Cai, Z. Wu, N. Lu, B. Yu, J. Zhang, C.F. Guo, Materials Today Physics. **2020**, 12,100191.

[168]. C. F. Guo, Y. Chen, L. Tang, F. Wang, Z. Ren, Nano Lett. **2016**, 16, 594–600.

[169]. S. Huang, Y. Liu, C. F. Guo, Z. Ren, Adv. Electron. Mater. **2017**, 3, 1600534.

[170]. J. Huang, L. Wang, Y. Jin, P. Lu, L.-L. Wang, N. Bai, G. Li, P. Zhu, Y. Wang, J. Zhang, Z. Wu, C. F. Guo, Adv. Funct. Mater. **2020**, 30, 2001518.

[171]. C. F. Guo, Q. Liu, G. Wang, Y. Wang, Z. Shi, Z. Suo, C.-W. Chu, Z. Ren, PNAS, **2015**, 112, 12332-12337.

[172]. C. F. Guo, Z. Ren, Materials Today, **2015**, 18, 143-154.

[173]. Y. Wang, C. Zhu, R. Pfattner, H. Yan, L. Jin, S. Chen, F. Molina-Lopez, F. Lissel, J. Liu, N. I. Rabiah, Z. Chen, J. W. Chung, C. Linder, M. F. Toney, B. Murmann, Z. Bao, Sci. Adv. **2017**, 3, e1602076.

[174]. D., Zhao, X., Wu, C., Guo, Inorg. Chem. Front. **2018**, 5, 1378-1385.

[175]. J. Li, S. Qi, J. Liang, L. Li, Y. Xiong, W. Hu, Q. Pei, ACS Appl. Mater. Interfaces, **2015**, 7, 14140.

[176]. Y. Wang, Y. Liu, C. Wang, H. Liu, J. Zhang, J. Lin, J. Fan, T. Ding, J. E. Ryu, Z. Guo, Engineered Science **2020**, 9, 50-59.

[177]. Y. Tian, X. Yang, A. Nautiyal, Y. Zheng, Q. Guo, J. Luo, X. Zhang, Adv Compos Hybrid Mater. **2019**, 2, 151–161.

[178]. I. Verboven, W. Deferme, Progress in Materials Science **2021**, 118, 100760.

[179]. L. Zhang, T. Song, L. Shi, N. Wen, Z. Wu, C. Sun, D. Jiang, Z. Guo, J Nanostruct Chem. **2021**, 11, 323–341.

[180]. H. S. Das, G. Roymahapatra, P. K. Nandi, R. Das, ES Energy & Environment **2021**, 13, 50-56.

[181]. W. Zhang, Q. Liu, P. Chen, Materials **2018**, 11, 1836.

[182]. S. Han, S. Hong, J. Ham, J. Yeo, J. Lee, B. Kang, P. Lee, J. Kwon, S. S. Lee, M.-Y. Yang, S. H. Ko, Adv. Mater. **2014**, 26, 5808.

[183]. P. Lee, J. Lee, H. Lee, J. Yeo, S. Hong, K. H. Nam, D. Lee, S. S. Lee, S. H. Ko, Adv. Mater. **2012**, 24, 3326.

[184]. Y. Wang, Q. Liu, J. Zhang, T. Hong, W. Sun, L. Tang, E. Arnold, Z. Suo, W. Hong, Z. Ren, C. F. Guo, Adv. Mater. **2019**, 31, 1902955.

[185]. C. F. Guo, T. Sun, Q. Liu, Z. Suo, Z. Ren, Nat. Commun. **2014**, 5, 3121.

[186]. H. Wu, D. Kong, Z. Ruan, P.-C. Hsu, S. Wang, Z. Yu, T. J. Carney, L. Hu, S. Fan, Y. Cui, Nat. Nanotechnol. **2013**, 8, 421.

[187]. S. Ding, J. Jiu, Y. Tian, T. Sugahara, S. Nagao, K. Suganuma, Phys. Chem. Chem. Phys. **2015**, 17, 31110.

[188]. Y. Liu, J. Zhang, H. Gao, Y. Wang, Y. Wang, Q. Liu, S. Huang, C. F. Guo, Z. Ren, Nano Lett. **2017**, 17, 1090–1096.

[189]. S. Zhang, B. Wang, J. Jiang, K. Wu, C. F. Guo, Z. Wu, ACS Appl. Mater. Interfaces **2019**, 11, 7148–7156.

[190]. B. Wang, W. Xin, K. Hjort, C. F. Guo, Z. Wu, ACS Appl. Polym. Mater. **2019**, 1, 145-151.

[191]. B. Wang, K. Wu, K. Hjort, C. Guo, Z. Wu, Soft Robotics. **2019**, 3, 414-421.

[192]. M. Shin, J. H. Song, G. H. Lim, B. Lim, J. J. Park, U. Jeong, Adv. Mater. **2014**, 26, 3706.

[193]. J. H. Song, Y. T. Kim, S. Cho, W. J. Song, S. Moon, C. G. Park, S. Park, J. M. Myoung, U. Jeong. Adv. Mater. **2017**, 29, 1702625.

[194]. Y. Tian, C. F. Guo, J. Zhang, Q. Liu, Phys. Chem. Chem. Phys. **2015**, 17, 851-857.

[195]. M. Krajewski, P.-Y. Liao, M. Michalska, M. Tokarczyk, J.-Y. Lin, Journal of Energy Storage **2019**, 26, 101020.

[196]. S. Huang, C.F. Guo, X. Zhang, W. Pan, X. Luo, C. Zhao, J. Gong, X. Li, Z.F. Ren, H. Wu, Small, **2015**, 11, 5712-5718.

[197]. S. Wang, J. Xu, W. Wang, G.-J. N. Wang, R. Rastak, F. Molina-Lopez, J. W. Chung, S. Niu, V. R. Feig, J. Lopez, T. Lei, S.-K. Kwon, Y. Kim, A. M. Foudeh, A. Ehrlich, A. Gasperini, Y. Yun, B. Murmann, J. B.-H. Tok, Z. Bao, Nature **2018**, 555, 83.

[198]. C. Feng, K. Liu, J. - S. Wu, L. Liu, J. - S. Cheng, Y. Zhang, Y. Sun, Q. Li, S. Fan, K. Jiang, Adv. Funct. Mater. **2010**, 20, 885-891.

[199]. K. Liu, Y. Sun, P. Liu, X. Lin, S. Fan, K. Jiang, Adv. Funct. Mater. **2011**, 21, 2721-2728.

[200]. Y. Zhang, C. J. Sheehan, J. Zhai, G. Zou, H. Luo, J. Xiong, Y. T. Zhu, Q. X. Jia, Adv. Mater. **2010**, 22, 3027.

[201]. F. Xu, X. Wang, Y. Zhu, Y. Zhu, Adv. Funct. Mater. **2012**, 22, 1279-1283.

[202]. X. Zhang, K. S. Ziemer, B. L. Weeks, Adv Compos Hybrid Mater. **2019**, 2, 492–500.

[203]. B. Zou, Y. Chen, Y. Liu, R. Xie, Q. Du, T. Zhang, Y. Shen, B. Zheng, S. Li, J. Wu, W. Zhang, W. Huang, X. Huang, F. Huo, Adv. Sci. **2019**, 6, 1801283.

[204]. T. Chen, Y. Xue, A. K. Roy, L. Dai, ACS Nano **2014**, 8, 1039.

[205]. G. Li, Z. Qiu, Y. Wang, Y. Hong, Y. Wan, J. Zhang, J. Yang, Z. Wu, W. Hong, C. F. Guo, ACS Appl. Mater. Interfaces **2019**, 11, 10373–10379.

[206]. M. Aleksandrova, V. Videkov, R. Ivanova, A. K. Singh, G. S. Thool. Materials Letters. **2016**, 174, 204-208.

[207]. S. u. Rehman, R. Ahmed, K. Ma, S. Xu, T. Tao, M. A. Aslam, M. Amir, J. Wang, Engineered Science **2021**, 13, 71-78.

[208]. M. Vosgueritchian, D. J. Lipomi, Z. Bao. Adv. Funct. Mater. **2012**, 22, 421.

[209]. M. W. Lee, M. Y. Lee, J. C. Choi, J. S. Park, C. K. Song, Org. Elec-tron. **2010**, 11, 854.

[210]. Q. Li, M. Deng, S. Zhang, D. Zhao, Q. Jiang, C.-F. Guo, Q. Zhou, W. Liu, J. Mater. Chem. C, **2019**, 7, 4374-4381.

[211]. J. H. Oh, P. Wei, Z. Bao, Appl. Phys. Lett.**2010**, 97, 243305.

[212]. D. J. Lipomi, J. A. Lee, M. Vosgueritchian, B. C. K. Tee, J. A. Bolander, Z. Bao, Chem. Mater.**2012**, 24, 373.

[213]. D. Y. Choi, H. W. Kang, H. J. Sung, S. S. Kim, Nanoscale **2013**, 5, 977.

[214]. Z. Wang, X. Li, L.Wang, Y. Li, J. Qin, P. Xie, Y. Qu, K. Sun, R. Fan, Adv Compos Hybrid Mater. **2020**, 3, 1–7.

[215]. Q. Gao, Y. Pan, G. Zheng, C. Liu, C. Shen, X. Liu, Adv Compos Hybrid Mater. **2021**, 4, 274–285.

[216]. H. Cheng, Y. Pan, Q. Chen, R. Che, G. Zheng, C. Liu, C. Shen, X. Liu, Adv Compos Hybrid Mater. **2021**, 4, 505–513.

[217]. C. F. Guo, Y. Lan, T. Sun, Z. Ren, Nano Energy, **2014**, 8, 110-117.

[218]. H. Charaya, T.-G. La, J. Rieger, H.-J. Chung, Adv. Mater. Technol. **2019**, 4, 1900327.

[219]. C. Keplinger, J.-Y. Sun, C. C. Foo, P. Rothemund, G. M. Whitesides, Z. Suo, Science **2013**, 341, 984.

[220]. Y. Cao, Y. J. Tan, S. Li, W. W. Lee, H. Guo, Y. Cai, C. Wang, B. C. K. Tee, Nat. Electron. **2019**, 2, 75.

[221]. H. Wang, B. Zhu, W. Jiang, Y. Yang, W. R. Leow, H. Wang, X. Chen, Adv. Mater. **2014**, 26, 3638.

[222]. H. Sun, X. You, Y. Jiang, G. Guan, X. Fang, J. Deng, P. Chen, Y. Luo, H. Peng, Angew. Chem., Int. Ed. **2014**, 53, 9526.

[223]. S. Park, G. Thangavel, K. Parida, S. Li, P. S. Lee, Adv. Mater. **2019**, 31, 1805536.

[224]. P. Chen, X. Sun, H. Peng, Adv. Funct. Mater. **2018**, 30, 2001827.

[225]. C. M. Boutry, A. Nguyen, Q. O. Lawal, A. Chortos, S. R. Gagne, Z. Bao, Adv. Mater. **2015**, 27, 6954.

[226]. Y. Luo, J. Shao, S. Chen, X. Chen, H. Tian, X. Li, L. Wang, D. Wang, B. Lu, ACS Appl. Mater. Interfaces **2019**, 11, 17796.

[227]. J. Yang, S. Luo, X. Zhou, J. Li, J. Fu, W. Yang, D. Wei, ACS Appl. Mater. Interfaces **2019**, 11, 14997-15006.

[228]. X. Shuai, P. Zhu, W. Zeng, Y. Hu, X. Liang, Y. Zhang, R. Sun, C. P. Wong, ACS Appl. Mater. Interfaces **2017**, 9, 26314.

[229]. X. Zeng, Z. Wang, H. Zhang, W. Yang, L. Xiang, Z. Zhao, L. M. Peng, Y. Hu, ACS Appl. Mater. Interfaces **2019**, 11, 21218.

[230]. S. H. Cho, S. W. Lee, S. Yu, H. Kim, S. Chang, D. Kang, I. Hwang, H. S. Kang, B. Jeong, E. H. Kim, S. M. Cho, K. L. Kim, H. Lee, W. Shim, C. Park, ACS Applied Materials & Interfaces **2017,** 9, 10128-10135.

[231]. Y. Wei, S. Chen, Y. Lin, Z. Yang, L. Liu, J. Mater. Chem. C, **2015**, 3, 9594.

[232]. Q. Chen, H. Tang , J. Liu , R. Wang , J. Sun , J Yao , Z. Shao , X. Chen, Chemical Engineering Journal Peng, **2021**, 422, 130091.

[233]. Y. Wan, Z. Qiu, Y. Hong, Y. Wang, J. Zhang, Q. Liu, Z. Wu, C. F. Guo, Adv. Electron. Mater. **2018**, 4, 1700586.

[234]. Q. Zou , Z. Lei , T. Xue , S. Li , Z. Ma , Q. Su, Sensors and Actuators A **2020**, 313, 112218.

[235]. N. Bai, L. Wang, Q. Wang, J. Deng, Y. Wang, P. Lu, J. Huang, G. Li, Y. Zhang, J. Yang, K. Xie, X. Zhao, C. F. Guo, Nat Commun **2020**, 11, 209.

[236]. G. Zhao, X. Zhang, X. Cui, S. Wang, Z. Liu, L. Deng, A. Qi, X. Qiao, L. Li, C. Pan, Y. Zhang, L. Li, ACS Appl. Mater. Interfaces **2018**, 10, 15855–15863.

[237]. X. Pan, Q. Wang, R. Guo, S. Cao, H. Wu, X. Ouyang, F. Huang, H. Gao, L. Huang, F. Zhang, L. Chen, Y. Ni, K. Liu, J. Mater. Chem. A, **2020**, 8, 17498.

[238]. B. Nie, R. Li, J. D. Brandt, T. Pan, Lab Chip, **2014**, 14, 4344.

[239]. D. Choi, S. Jang, J. S. Kim, H. J. Kim, D. H. Kim, J. Y. Kwon, Adv. Mater. Technol. **2019**, 4, 1800284.

[240]. L. Cai, G. Chen, J. Tian, B. Su, M. He, Chem. Mater. **2021**, 33, 2072−2079.

[241]. P. Lu, L. Wang, P. Zhu, J. Huang, Y. Wang, N. Bai, Y. Wang, G. Li, J. Yang, K. Xie, J. Zhang, B. Yu, Y. Dai, C. F. Guo, Science Bulletin, **2021**, 66, 1091-1100

[242]. H. Chen, Y. Gao, X. Ren, G. Gao, Carbohydrate Polymers **2020**, 235, 116018.

[243]. M. O. Cicek, D. Doganay, M. B. Durukan, M. C. Gorur, H. E. Unalan, Adv. Mater. Technol. **2021**, 6, 2001168.

[244]. S. Kim, M. Amjadi, T. Lee, Y. Jeong, D. Kwon, M. S. Kim, K. Kim, T. Kim, Y. S. Oh, ACS Appl. Mater. Interfaces **2019**, 11, 23639−23648.

[245]. L. Dai, J. Lu, F. Kong, K. Liu, H. Wei, C. Si, Adv Compos Hybrid Mater. **2019**, 2, 462–470.

[246]. Q. Lin, J. Huang, J. Yang, Y. Huang, Y. Zhang, Y. Wang, J. Zhang, Y. Wang, L. Yuan, M. Cai, X. Hou, W. Zhang, Y. Zhou, S. Chen, C. F. Guo, Adv. Healthcare Mater. **2020**, 9, 2001023.

[247]. L. Pan, A. Chortos, G. Yu, Y. Wang, S. Isaacson, R. Allen, Y. Shi, R. Dauskardt, Z. Bao, Nat. Commun. **2014**, 5, 3002.

[248]. D. Kwon, T. Lee, J. Shim, S. Ryu, M. S. Kim, S. Kim, T. Kim, I. Park, ACS Applied Materials & Interfaces **2016**, 8, 16922-16931.

[249]. W. Zhong, Q. Liu, Y. Wu, Y. Wang, X. Qing, M. Li, K. Liu, W. Wang, D. Wang, Nanoscale **2016**, 8, 12105.

[250]. J. C. Yang, J. O. Kim, J. Oh, S. Y. Kwon, J. Y. Sim, D. W. Kim, H. B. Choi, S. Park, ACS Appl. Mater. Interfaces **2019**, 11, 19472.

[251]. W. Qiu, C. Zhang, G. Chen, H. Zhu, Q. Zhang, S. Zhu, ACS Appl. Mater. Interfaces **2021**, 13, 26490 − 26497.

[252]. V. Amoli, J. S. Kim, E. Jee, Y. S. Chung, S. Y. Kim, J. Koo, H. Choi, Y. Kim, D. H. Kim, Nat. Commun. **2019**, 10, 4019.

[253]. S. Burattini, B. W. Greenland, D. H. Merino, W. Weng, J. Seppala, H. M. Colquhoun, W. Hayes, M. E. Mackay, I. W. Hamley, S. J. Rowan, J. AM. CHEM. SOC. **2010**, 132, 12051–12058.

[254]. Z. Wei, J. H. Yang, J. Zhou, F. Xu, M. Zrınyi, P. H. Dussault, Y. Osada, Y. M. Chen, Chem. Soc. Rev. **2014**, 43, 8114.

[255]. J. S. Kim, H. Choi, H. J. Hwang, D. Choi, D. H. Kim, Macromol. Biosci. **2020**, 20, 2000147.

[256]. X. Pu, M. Liu, X. Chen, J. Sun, C. Du, Y. Zhang, J. Zhai, W. Hu, Z. L. Wang, Sci. Adv. **2017**, 3, e1700015.

[257]. C. Pang, G.-Y. Lee, T.-il Kim, S. M. Kim, H. N. Kim, S.-H. Ahn, K.-Y. Suh, Nature Mater **2012**, 11, 795–801.

[258]. Z. Zhu, Y. Wang, X. Hu, X. Sun, L. Chang, P. Lu, Appl. Phys. Lett. **2016**, 109, 073504.

[259]. M. Zirkl, A. Sawatdee, U. Helbig, M. Krause, G. Scheipl, E. Kraker, P.A. Ersman, D. Nilsson, D. Platt, P. Bodö, S. Bauer, G. Domann, B. Stadlober, Adv. Mater. **2011**, 23, 2069-2074.

[260]. K. Takei, T. Takahashi, J. C. Ho, H. Ko, A. G. Gillies, P. W. Leu, R. S. Fearing, A. Javey, Nature Mater **2010**, 9, 821–826.

[261]. Y. Wang, J. Wang, M. Hao, B. Li, Z. Zhu, X. Gou, L. Li, RSC Adv. **2020**, 10, 27447.

[262]. S. Yamada, H. Toshiyoshi, ACS Appl. Mater. Interfaces **2020**, 12, 36449−36457.

[263]. N. Jiang, H. Li, D. Hu, Y. Xu, Y. Hu, Y. Zhu, X. Han, G. Zhao, J. Chen, X. Chang, M. Xi, Q. Yuan, Composites Communications, **2021**, 27, 100845.

[264]. C. M. Boutry, M. Negre, M. Jorda, O. Vardoulis, A. Chortos, O. Khatib, Z. Bao, Sci. Rob. **2018**, 3, eaau6914.

[265]. J. Park, J. Kim, J. Hong, H. Lee, Y. Lee, S. Cho, S.-W. Kim, J. J. Kim, S. Y. Kim, H. Ko, NPG Asia Mater. **2018**, 10, 163.

[266]. A. Atalay, V. Sanchez, O. Atalay, D. M. Vogt, F. Haufe, R. J. Wood, C. J. Walsh, Adv. Mater. Technol. **2017**, 2, 1700136.

[267]. O. Atalay, A. Atalay, J. Gafford, H. Wang, R. Wood, C. Walsh, Adv. Mater. Technol. **2017**, 2, 1700081.

[268]. J. Eom, R. Jaisutti, H. Lee, W. Lee, J. Heo, J. Lee, S. Park, Y. Kim, ACS Appl. Mater. Interfaces **2017**, 9, 10190−10197

[269]. J. Shintake, E. Piskarev, S. H. Jeong, D. Floreano, Adv. Mater. Technol. **2018**, 3, 1700284.

[270]. J. Lee, H. Kwon, J. Seo, S. Shin, J.H. Koo, C. Pang, S. Son, J.H. Kim, Y.H. Jang, D.E. Kim, T. Lee, Adv. Mater. **2015**, 27, 2433-2439.

[271]. J. Hashizume, T. M. Huh, S. A. Suresh, M. R. Cutkosky, IEEE Robot. Autom. Lett. **2019**, 4, 677.

[272]. R. P. Rocha, P. A. Lopes, A. T. De Almeida, M. Tavakoli, C. Majidi, J. Micromech. Microeng. **2018**, 28, 034001.

[273]. Y. Qian, Y. Zhou, M. Lu, X. Guo, D. Yang, H. Lou, X. Qiu, C. F. Guo, Small Methods **2021**, 5, 2001311.

[274]. S. Sharma, A. Chhetry, S. Zhang, H. Yoon, C. Park, H. Kim, Md. Sharifuzzaman, X. Hui, J. Y. Park, ACS Nano **2021**, 15, 4380−4393.

[275]. G. Gu, H. Xu, S. Peng, L. Li, S. Chen, T. Lu, X. Guo, Soft Robotics **2019**, 6, 368-376.

[276]. N. Ni. Alexandria Engineering Journal **2021**, 60, 5991-6000.

[277]. J. Li, R. Bao, J. Tao, Y. Peng, C. Pan, J. Mater. Chem. C, **2018**, 6, 11878-11892.

[278]. S. Li, X. Xiao, J. Hu, M. Dong, Y. Zhang, R. Xu, X. Wang, J. Islam, ACS Appl. Electron. Mater. **2020**, 2, 2282−2300

[279]. B. Zhuo, S. Chen, M. Zhao, X. Guo, IEEE J. Electron Devices Soc. **2017**, 5, 219.

[280]. H. Ouyang, J. Tian, G. Sun, Y. Zou, Z. Liu, H. Li, L. Zhao, B. Shi, Y. Fan, Y. Fan, Z. Wang, Z. Li, Adv. Mater. **2017**, 29, 1703456.

[281]. S. M. Khan, N. Qaiser, S. F. Shaikh, M. M. Hussain, IEEE Trans. Electron Devices **2020**, 67, 249.

[282]. S. Sharma, A. Chhetry, M. Sharifuzzaman, H. Yoon, J. Y. Park, ACS Appl. Mater. Interfaces **2020**, 12, 22212.

[283]. G. J. Jeon, H. I. Yeom, T. Jin, J. Kim, J. Yang, S. H. K. Park, J. Mater. Chem. C **2020**, 8, 4271.

[284]. Y. Lee, J. Park, S. Cho, Y. E. Shin, H. Lee, J. Kim, J. Myoung, S. Cho, S. Kang, C. Baig, H. Ko, ACS Nano **2018**, 12, 4045.

[285]. C. Deng, W. Tang, L. Liu, B. Chen, M. Li, Z. L. Wang, Adv. Funct. Mater. **2018**, 28, 1801606.

[286]. S. W. Park, P. S. Das, J. Y. Park, Org. Electron. **2018**, 53, 213.

[287]. J. Tao, M. Dong, L. Li, C. Wang, J. Li, Y. Liu, R. Bao, C. Pan, Microsyst. Nanoeng. **2020**, 6, 1.

[288]. Z. Zhang, Z. Zhu, B. Bazor, S. Lee, Z. Ding, T. Pan, IEEE Trans. Biomed. Eng. **2019**, 66, 3072.

[289]. Y. Wang, S. Gong, S. J. Wang, G. P. Simon, W. Cheng, Mater. Horiz.**2016**, 3, 208.

[290]. S. G. Yoon, H.-J. Koo, S. T. Chang, ACS Appl. Mater. Interfaces **2015**, 7, 27562.

[291]. P. Wang, G. Li, J. Liu, Z. Hou, C. Meng, S. Guo, ACS Applied Electronic Materials **2021**, 3, 2195-2202.

[292]. Y. Xiao, Y. Duan, N. Li, L. Wu, B. Meng, F. Tan, Y. Lou, H. Wang, W. Zhang, Z. Peng, ACS Sensors **2021**, 6, 1785-1795.

[293]. R. Fu, Y. Yang, C. Lu, Y. Ming, X. Zhao, Y. Hu, L. Zhao, J. Hao, W. Chen, ACS Omega **2018**, 3, 9146−9154.

[294]. K.-Y. Chun, Y. J. Son, C.-S. Han, ACS Nano **2016**, 10, 4550.

[295]. D. S. Song, D. G. Han, K. Rhee, D. M. Kim, J. Y. Jho, Macromol. Res. **2017**, 25, 1205-1211.

Zhao Chun is currently a Ph.D. candidate under the supervision of Prof. Yanjie Wang of Hohai University, Jiangsu Province, China. He obtained a master's degree from College of Mechanical & Electrical Engineering, Hohai University in 2020. His research interests mainly focus on control system and robot technology, flexible sensors and soft robots.

Yanjie Wang is currently working as a professor in College of Mechanical and electrical Engineering, Hohai University, Jiangsu Province, China. He received his PH.D. degree in Mechanical Engineering from Xi'an Jiaotong University (XJTU), Xi'an, China, in 2015. His research interests include smart materials and structures, advanced bionic system and robot technology, micro actuation/sensing technology.

Chuanfei Guo is currently working as a professor in the department of Materials Science and Engineering, Southern University of Science and Technology, Shenzhen, China. He joined Southern University of Science and Technology in 2016. His research interests include high-performance electronic skin, flexible electronic technology, and micro sensing technology.

Lijie Li is currently working as professor in college of engineering, Swansea University, UK. He received his Ph.D. degree in electrical and electronics from the University of Strathclyde, UK in 2004. His research areas mainly include energy harvesting, RF, optical micro-nano sensors and actuators.